SYNTHESIS AND MULTIFERROIC PROPERTIES OF $Bi_{3.4}M_{0.6}Ti_3O_{12}/CoFe_2O_4$ (M= La^{3+} and Sm^{3+}) MULTILAYER STRUCTURES

by

Amanda E. Charris-Hernández

A thesis submitted in partial fulfillment of the requirements for the degree of

MASTER OF SCIENCE

in

PHYSICS

UNIVERSITY OF PUERTO RICO

MAYAGÜEZ CAMPUS

2013

Approved by:

_____	_____
Maharaj S. Tomar, Ph. D President, Graduate Committee	Date
_____	_____
Dorial Castellanos-Rodríguez, Ph. D Member, Graduate Committee	Date
_____	_____
Sergiy Lysenko, Ph. D Member, Graduate Committee	Date
_____	_____
Gladys O. Ducoudray, Ph. D Representative of Graduate Studies	Date
_____	_____
Rafael Ramos, Ph. D Chairperson of the Department	Date

ABSTRACT

In search of new multiferroic materials $Bi_{4-x}M_xTi_3O_{12}$ and $CoFe_2O_4$ alternate layers were investigated. For this work, multilayer films of $Bi_{3.4}M_{0.6}Ti_3O_{12}$ with M = La^{3+}, Sm^{3+} and $CoFe_2O_4$ were synthesized by chemical solution method and deposited by spin coating processing on Pt (Pt/Ti/SiO_2/Si) substrate and annealed at 750 °C under oxygen atmosphere, because both materials reach at 750 ºC their formation phase.

Multilayers were investigated by X-ray diffraction and Scanning electron microscopy (SEM). X-ray patterns for pure $CoFe_2O_4$, $Bi_{3.4}M_{0.6}Ti_3O_{12}$ and $Bi_{3.4}Sm_{0.6}Ti_3O_{12}$ confirm the formation of the spinel and perovskite structures respectively. On the other hand the presence of the predominant peaks (006), (117) of $Bi_4Ti_3O_{12}$ and (311), (511) of $CoFe_2O_4$ in all the multilayers revealed the composite-like structure. Multilayer show large values in spontaneous ferroelectric polarization and ferromagnetic memory with well-saturated hysteresis loop, confirming composite behavior of the material. The better polarization values were observed in films that exhibit a preferential orientation in the c-axis as well as in those films with layers of $Bi_{4-x}M_xTi_3O_{12}$ thicker. The leakages current were below 10^{-5} A for most samples, and the dielectric response showed clear relaxation in the frequency range 10^{-2} – 10^{-6} Hz. The relaxation seems to reflect on the ferroelectric and ferromagnetic responses.

The co-existence of ferroelectric and ferromagnetic in alternate $Bi_{3.4}M_{0.6}Ti_3O_{12}$/$CoFe_2O_4$ (M= La and Sm) layers is attributed to the stress in the composite material, due to different permittivity and permeability of the materials involved.

RESUMEN

Se investigó capas alternas de $Bi_{4-x}M_xTi_3O_{12}$ y $CoFe_2O_4$ en la búsqueda de nuevos materiales multiferroico. En este trabajo se prepararon películas delgadas en forma de multicapas del sistema $Bi_{3.4}M_{0.6}Ti_3O_{12}$ con M= La^{3+}, Sm^{3+} para y $CoFe_2O_4$ depositadas sobre sustratos de Platino ($Pt/Ti/SiO_2/Si$) preparadas por un sencillo método de solución química y depositadas con la técnica *spin-coating*, y tratadas térmicamente a 750ºC bajo atmosfera de oxígeno, a esta temperartura ambos materiales llegan a su fase de formación.

Las multicapas fueron investigadas por difracción de rayos X y Microscopia Electrónica de Barrido (SEM). Los patrones de difracción para películas puras de $CoFe_2O_4$, $Bi_{3.4}La_{0.6}Ti_3O_{12}$ y $Bi_{3.4}Sm_{0.6}Ti_3O_{12}$ confirman la formación de las estructuras espinela y perovskite respectivamente. Por otro lado la presencia de los picos más intensos (006), (117) de $Bi_4Ti_3O_{12}$ y (311), (511) $CoFe_2O_4$ en todas las multicapas revelan la formación de una estructura compuesta.

Las multicapas muestran valores altos en la polarización ferroeléctrica espontánea y memoria ferromagnética con ciclos de histéresis bien saturados, confirmando que es un material compuesto. Los mejores valores en la polarización se observaron en las películas que muestran una orientación preferencial en el eje c, así como en aquellas películas con capas de $Bi_{4-x}M_xTi_3O_{12}$ más gruesas. La pérdida de corriente está por debajo de 10^{-5} A para todas las muestras, y la respuesta dieléctrica mostró una clara relajación en un rango de frecuencia de 10^{-2} – 10^{-6} Hz. La relajación aparece reflejada en la respuesta ferroeléctrica y ferromagnética.

La co-existencia ferroeléctrica y ferromagnética en capas alternas de $Bi_{4-x}M_xTi_3O_{12}$/ $CoFe_2O_4$ (M = La, Sm) es atribuido al estrés en el material compuesto, debido a los diferentes valores de permitividad y permeabilidad de los materiales envueltos.

DEDICATORY

To my lovely mother Sonia Hernández, that gave everything to me

To my brothers Jonathan and Daimer, for inspiring me

To my friend Gary, for his love

A mi madre Sonia Hernández, que me ha dado todo

A mis hermanos Jonathan y Daimer, por inspirarme

A mi gran amigo Gary, por su amor

ACKNOWLEDGMENTS

Thank God who is living inside me.

Special thanks to the University of Puerto Rico at Mayagüez for giving me the amazing opportunity to develop myself as a student, teacher and researcher.

- Thanks to my advisor Professor Maharaj. S. Tomar for his support, motivation, and the opportunity to work in his laboratory.
- Thanks to Dr. Ricardo Melgarejo for his help and his unconditional disposition.
- Thanks to M. S. Danilo Barrionuevo for their support in the measurements.
- Thanks to Dr. Ram Katiyar for facilitating their equipment to make the measurements.
- Thanks to Dr. A. Kumar for his help in calibration of the chemical balance.
- Thanks to Delva Rivera and Juan Santiago for facilitating thickness measure.
- Special thanks to my colleagues Renny Nazario and Armando Peña for their friendship and cooperation.
- Special thanks to Andres Velázquez for his hospitality.
- The graduate fellowship from DoE-EPSCOR grant #DE-FG-02-08ER46526 is gratefully appreciated.

TABLE OF CONTENTS

FIGURE LIST

TABLE LIST

I. INTRODUCTION

Co-existence of ferroelectric and ferromagnetic responses in the same material and magneto-electric couplings at room temperature is important for new memory devices. The unusual properties and fascinating underlying physics could lead to new devices such as coupled FeRAMs (ferroelectric random access memories) and MRAMs (magnetic random access memories), non-linear magneto-optical, surface acoustic wave devices, tunable capacitors, and sensing applications [1]. Magnetoelectrics materials were studied to some degree in the 1960s and 1970s but then weakened in large part because single-phase materials with both properties could not be extensively produced. The reawakening has been continued by means of the development of new types of compound with electrical and magnetic properties. Advances in thin-films growth techniques have provided formation of structures and phases which are necessary for magneto-electrical coupling.

Aurivillious phase compound system consists of $(Bi_2O_2)^{2+}$ $(A_{n-1}\,B_nO_{3n+1})^{2-}$, where A is mono, di, or trivalent cations, B is cation with valence 4, 5 or 6, and n is the number of perovskite layers [2], [3]. $Bi_4Ti_3O_{12}$ is one of compound of Aurrivillious family of monoclinic ferroelectric structure with one component of polarization in the plane of the layers and the other component perpendicular to this plane and shows low ferroelectric polarization [4]–[6]. The Bi^{3+} ions in A-site can be partially substituted by trivalent cation to form a solid solution of the type $Bi_{4-x}M_xTi_3O_{12}$ (M = trivalent cation, such as La^{3+}, Nd^{3+}, Sm^{3+} etc.) which tend to gradually alter the crystal structure. Such structures have shown large spontaneous ferroelectric polarization. $BaTiO_3$ is perovskite ferroelectric and $CoFe_2O_4$ is well known ferrimagnetic material with spinel

structure. $BaTiO_3$-$CoFe_2O_4$ alternate layers in multilayer structures are prepared by pulsed laser deposition (PLD). These have been investigated in order to study the ferroelectric (FE) and ferromagnetic (FM) coupling [7] and Stoichiometric phase formation of the involving materials at the same temperature is essentially required.

$Bi_{4-x}Nd_xTi_3O_{12}/CoFe_2O_4$ composite like multilayer have also been investigated [5], [8]. However, due to the improper phase formation of the bilayer structure, responses were poor. For a better understanding of the structure and properties, we work to multilayer structures synthesized by chemical solution route and deposited by spin-coating processing.

$Bi_{3.4}M_{0.6}Ti_3O_{12}/CoFe_2O_4$ (M= La and Sm) multilayer were deposited by spin coating on Pt substrate ($Pt/TiO_2/SiO_2/Si$). We report here the structural, dielectric, leakage current responses, and the magneto-electric properties of the multilayer structures at room temperature.

Aim of study

Main objective

Investigate magneto-electric coupling of bismuth ferrite $Bi_{4-x}M_xTi_3O_{12}$ (M= La, Sm, Nd) perovskite structure and cobalt ferrite $CoFe_2O_4$ spinel structure in multilayer films deposited in Pt ($Pt/Ti/SiO_2/Si$) substrate with a simple method and spin-coating processing.

Specific objectives

- ✓ Determine the effect to different substituted ions in bismuth (La^{3+} and Sm^{3+}) and its composition (x=0.6) on the ferroelectric and ferromagnetic properties.

- ✓ Determine the relationship between ferroelectric and ferromagnetic responses related with the amount of layers deposited.

II. THEORETICAL BACKGROUND

2.1 Magnetism effect

The magnetic properties of solids originate in the motion of the electrons and in the permanent magnetic moments of the atoms and electrons. Magnetic properties are often in terms of the susceptibility χ; this is defined in terms of the magnetic moment m_m produced by a magnetic intensity $\boldsymbol{H}$, as

$$\chi_v = \frac{m_m}{H} \qquad \textbf{(1)}$$

The susceptibility and the magnetic moment can be defined for a unit volume, unit mass, or a mole. Under an applied magnetic field the materials have a characteristic behavior and this is reflected in the value of the susceptibility, depending on the susceptibility value of magnetic materials is classified as:

(a) Diamagnetism, which is very weak, arises from changes in the atomic orbital states induced by the applied field, with susceptibility of the order of 10^{-5}. It can be observed only when all the other types of magnetism are totally absent.

(b) Paramagnetism, is the results of the presence of permanent atomic or electronic magnetic moments, with small but positive susceptibility of the order between 10^{-3} and 10^{-5}.

(c) Ferromagnetism, which is very strong, occurs when quantum mechanical exchange interactions align adjacent magnetic moments in the same direction. Atoms or ions that are neighboring or close by in a solid can communicate with each other so that, even in the absence of an applied magnetic field, atoms or ions within a limited volume have all their magnetic

moments oriented with respect to one another. This communications is a form of quantum-mechanical coupling called the exchange interaction. Examples of ferromagnetic materials include iron (Fe), cobalt (Co), nickel (Ni) and gadolinium (Gd). A region in which all atoms have magnetic moments in the same direction is called ferromagnetic domain. When no external magnetic field has been applied to a ferromagnetic material, the magnetic moments of various domains cancel one another, so the magnetic induction or magnetic flux density B is zero. In the presence of an external magnetic field ($H>0$), the domains with magnetic moments in the same direction as H grow while those with magnetic moment in other directions shrink. This process, which involves the shift of the domain boundaries and the rotation of the domains, results in $B>0$. The curve of B versus H is shown schematically in Figure 2.1. As the applied field, H, is increased B begins to increase slowly. Then, the slope rises sharply and B rapidly increases until the *saturation induction*, B_s, is attained. The slope levels off with further increase in the field. Upon decreasing the field, the original curve is not retraced. At H equal to zero, the specimen is still magnetized and $B = B_r$, the *remanent induction.* At $B = 0$, the field H is equal to the coercive field H_c. If H is now made negative and the specimen saturated in the reverse direction before returning to zero field, the symmetric curve is obtained with a saturation, coercive field, and remanence equal to those on the positive side. Such irreversible, valued *hysteresis loop* behavior is characteristic of the magnetic behavior of ferromagnetic materials. The work required to go around the *hysteresis loop* once is proportional to the area enclosed by the curve. If H is brought back to zero and the cycle repeated at less than saturation, then a similar hysteresis curve of smaller area is obtained.

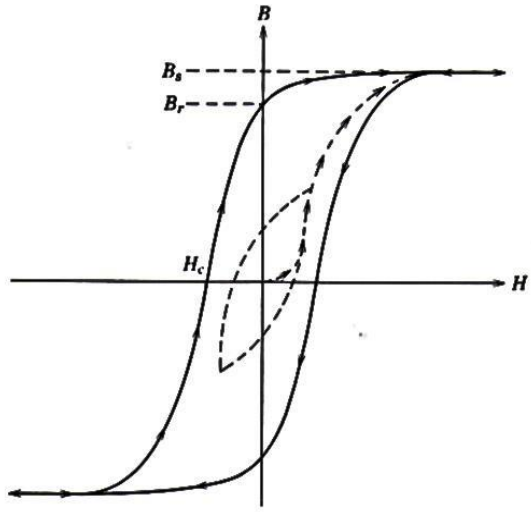

Figure 2. 1 *B versus H hysteresis loop for a ferromagnetic material. The dashed line indicates the behavior on initially increasing the applied field H.* [9]

(d) Antiferromagnetism, occurs when the spins are aligned oppositely rather than in the same direction and the vector sum of the magnetic moments of all the atoms in the domain is zero, the susceptibility is positive and increases as the temperature increases since the thermal energy disrupts the antiparallel moment arrangements and presents them to line up with the field [10].

(e) Ferrimagnetism, occurs when the atoms (or ions) having non zero magnetic moments within a ferromagnetic domain communicate with one another via a form of coupling (the magnetic atoms or ions are often separated by non-magnetic ions), so that the magnetic moment of every magnetic atom or ions in the domain, is in one of two anti-parallel directions and the vector sum of the magnetic moments of all these atoms or ions in the domain is not zero. Consequently a net moment result. The most common material which shows this behavior is magnetite, Fe_3O_4, which has a spinal structure. Materials which exhibit ferrimagnetism now all tend to be called ferrites even if they do not contain any iron. Ferrites are of great technical

importance because they have a very high electrical resistivity together with great magnetic permeability. When they are magnetized their behavior is very similar to that of ferromagnets, although the saturation value is not as large as in the ferromagnetic case. Ferrimagnetic materials have hysteresis curves like Figure 2.2 and domain structure is similar to those in ferromagnetic materials and their hysteresis curve made them very suitable for memory stores.

The peak in the χ versus $\boldsymbol{T}$ curve shown in Figure 2.3 for each magnetic behavior, for antiferromagnetic materials is called the *Neel temperature* Θ and corresponds to the Curie temperature in ferromagnetic materials [9].

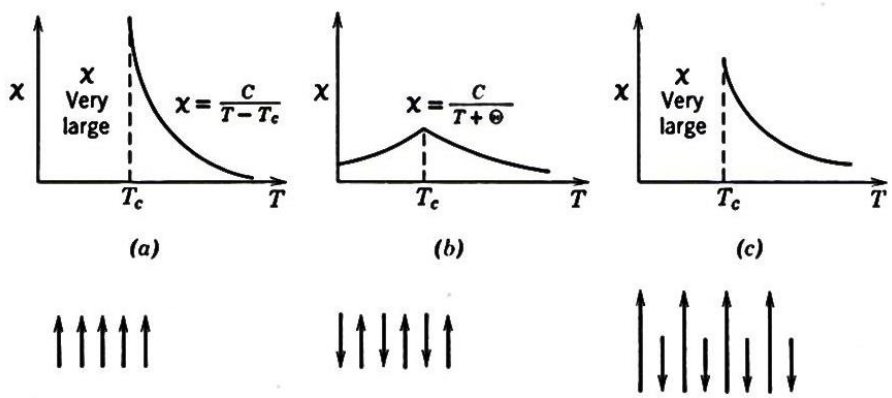

Figure 2. 2 *Magnetics susceptibility versus Temperature for (a) ferromagnetic, (b) antiferromagnetic, and (c) ferrimagnetic materials, with magnetic moment alignments indicated for each case*

2.2 Ferroelectricity effect

In Table 1.1 shows a list of various physical effects applied a material (electric field, magnetic field, stress, heat and light) and how are his responses (charge/current, magnetization, strain, temperature and light).

Table 1 *Various effects in materials* [11].

	CHARGE/CURRENT	MAGNETIZATION	STRAIN	TEMPERATURE	LIGHT
ELEC. FIELD	Permittivity Conductivity	Electromagnetic effect	Converse Piezo-effect	Caloric effect	Optic effect
MAG. FIELD	Magnetoelectrics effect	Permeability	Magnetostriction	Caloric effect	Optic effect
STRESS	Piezoelectric effect	Piezomagnetic effect	Elastic constant	--------	Photoelastic effect
HEAT	Pyroelectric effect	---------	Thermal expansion	Specific heat	--------
LIGHT	Photovoltaic effect	---------	Photostriction	---------	Refractive index

Are showed elastic materials, which generate current and strain outputs, respectively, for the input, voltage or stress. On the other hand, Pyroelectric and piezoelectric materials, which generate an electric field with the input of heat and stress, respectively, are called “smart” materials. Ferroelectric materials exhibit most of these effects with the exception of the magnetic phenomena, such as, magnetic field and magnetostriction.

Dielectric materials is one in which an electric dipole can be induced by applying an electric field. The electron clouds deform, causing electric dipoles; this phenomenon too is known as

electric polarization of the dielectric, and the polarization is expressed quantitatively as the sum of the electric dipoles per unit volume [C/m^2].

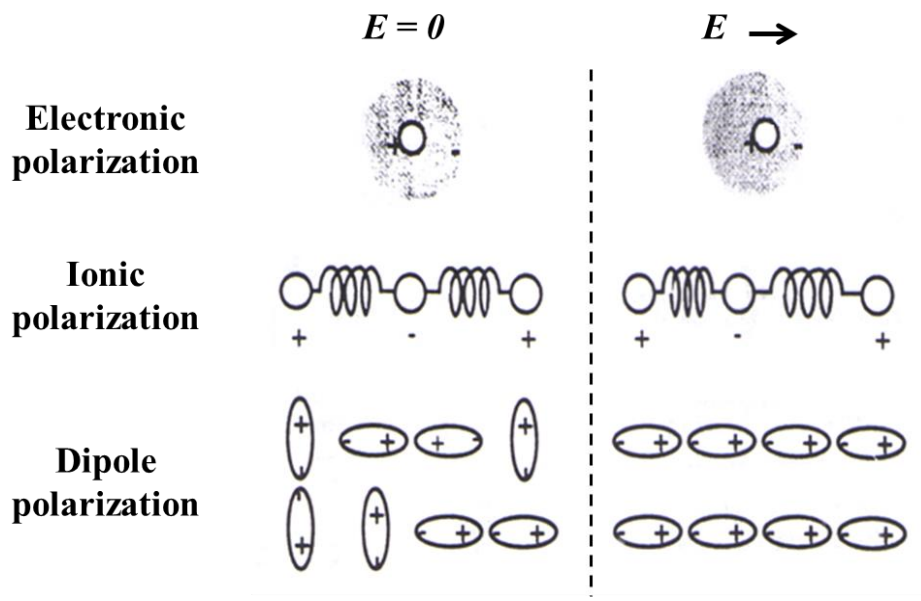

Figure 2. 3 *Microscopic origins of the electric polarization* [9]

Figure 2.4 shows the origin of the electric polarization. There are three primary contributions: Electronic polarization: occurs when an electric field acts on an individual atom. In zero fields the positively charged nucleus and the negative cloud of electrons are symmetrically disposed to one another and the atom has no dipole moment. When a field is applied the nucleus and the electrons move with respect to one another and the atom acquires a dipole moment ***p***, thus expressed:

$$\vec{p} = \alpha \vec{E} \quad \textbf{(2)}$$

Where α is the polarizability of the atom. This mechanism is operative in all dielectric materials. Ionic polarization: a second effect can arise with permanent dipoles. The field will tend to stretch the bonds between the ions and changes the moment of the molecule; an electric

field can shift the positive ion sub lattice relative to the negative ion sub lattice and this gives the crystal a dipole moment. Dipole polarization: if the system is composed of heteronuclear molecules then the disposition of the individual atoms within a molecule may be such that the molecule itself has a permanent dipole moment. In zero fields, the permanent dipoles will be randomly oriented and the system has no net polarization, but an electric field will tend to align the dipoles and the material will acquire a net moment. Due to the randomizing effect of the thermal vibrations this type of polarization is more effective as the temperature is decreased and it gives rise to a dielectric constant which is temperature dependent. In solids, however, the molecules are usually so tightly bound that orientation polarization does not seem to occur. It is more important in liquids and gases. Each mechanism contributes to the overall polarization of the material and depends on the frequency of the applied field [11].

Depending on the crystal structure the centers of the positive and negative charges may not coincide without the application of an external electric field. Such crystals have a spontaneous polarization. When the spontaneous polarization of the dielectric can be reversed by an electric field, it is called *ferroelectric*, is important say not every dielectric is a ferroelectric. Depending on their geometry crystals are commonly classified into seven systems: triclinic (the least symmetrical), monoclinic, orthorhombic, tetragonal, trigonal, hexagonal and cubic. These systems can again be sub-divided into point groups (crystal classes) according to their symmetry with respect to a point. There are 32 such crystal classes, 11 possess a center of symmetry and the other 21 remaining classes not possess center of symmetry are called *piezoelectric*, because positive and negative charges are generated on the crystal surfaces when appropriate stresses are applied. Of the piezoelectric crystal classes, 10 show a unique polar axis these crystals are called *polar or pyroelectric* because they possess spontaneous polarization or electric moment per unit

volume. Frequently this spontaneous polarization cannot be detected by charges on the surface of the crystal; the depolarizing field which results from such a charge distribution can be compensated by the flow of free charge within the crystal and in the surrounding medium [12]. However, the spontaneous polarization in general temperature dependent and its existence can be detected by observing the flow of charge to and from the surfaces on change of temperature.

A material is said to be ferroelectric when it has two or more orientation states in the absence of an electric field and can be shifted from one to another of these states by an electric field. Any two of the orientation states are identical in crystal structure and differ only in electric polarization at zero applied fields. The ferroelectricity has a behavior ordinary dielectric (usually less than 100) when subject to a phase transition from high temperature to a low temperature a ferroelectric crystal shows a reversible spontaneous electric polarization and a hysteresis loop with dielectric constant up 10^5. This transition is delimited by a point called the Curie Temperature T_c. Figure 2.5 shows schematically the temperature dependence of the spontaneous polarization P_s and permittivity ε (dielectric constant) of the barium titanate $BaTiO_3$ (T_c = 120 ºC). P_s decreases with increasing temperature and vanishes at the Curie temperature, while ε tends to diverge near T_c. Also, the reciprocal permittivity 1/ε is known to be linear with respect to the temperature over a wide range in the paraelectric phase, so-called *Curie-Weiss law:*

$$\chi = \frac{C}{(T - T_0)} \quad \textbf{(3)}$$

Where ***C*** is the *Curie-Weiss constant* and T_0 is the *Curie-Weiss temperature*. T_0 is slightly lower than the exact transition temperature T_c.

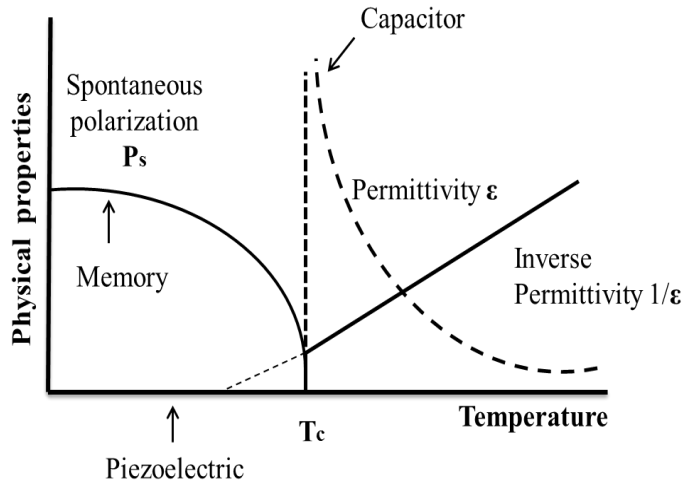

Figure 2. 4 *Spontaneous polarization and permittivity in ferroelectric materials dependence of the temperature*

Ferroelectrics have a large reversible spontaneous polarization, in response to an applied electrical field. In other words the ferroelectric material can have nonzero polarization in the absence of an applied electric field due to an orientation of microscopic-scale domains (regions in which the polarization is homogeneous). The mechanics of domain motion is simply the small shift of ion positions within unit cell, resulting in the net change of orientation. Such domain motion results in spontaneous polarization. Besides this, the direction of the spontaneous polarization can be reversed by applied field in opposite direction. Under applied field, unit cell dipole are orientations roughly parallel to the applied field in this case, domains with such orientations grow at the expenses of other, less favorably oriented. A ferroelectric hysteresis loop is the result of an alternating electric field. A typical hysteresis loop is shown in Figure 2.6 clearly the plot of polarization versus field does not retrace itself. A dashed line indicates the initial spontaneous polarization illustrated up to the saturation spontaneous P_s, is the polarization due to maximum domain growth, and is extrapolated to zero field (E = 0) to correct for the induced polarization not due to domain orientation.

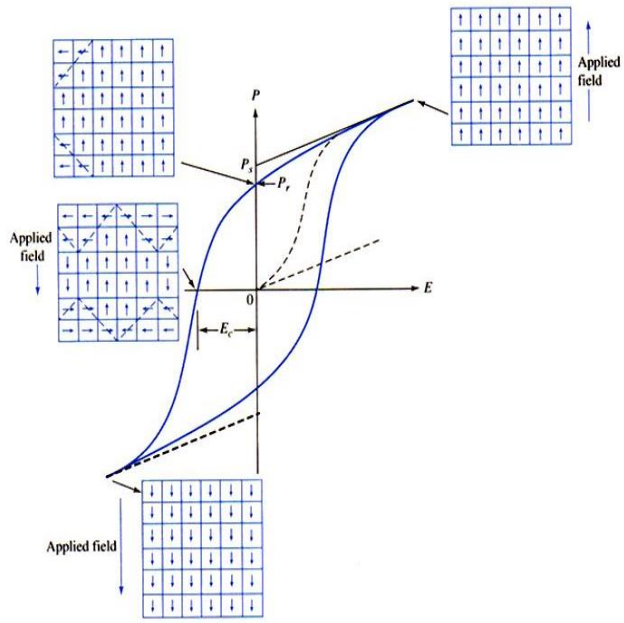

Figure 2. 5 *A ferroelectric hysteresis loop. Polarization versus electric field during first application of electric field (dashed curve) and during subsequent cycling of electric field (solid curve)*[9]

Upon decreasing E after reaching the saturation polarization, domains with dipole moments not in the same direction as E, appear again and they grow as E decreases. At the same time, domains with dipole moments in the same direction as electric field shrink. This process again involves the movement of domain boundaries. In spite of this tendency, P does not return all the way to zero when E returns to zero. The remnant polarization, P_r, is that remaining upon actual field removal $(P = P_r > 0)$ remains when $E = 0$. In order for polarization to return all the way to zero, an electric field must be applied in the reverse direction, the required electric field is $E = -E_c$, where E_c is called the coercive electrical field. The coercive field should be sufficiently high for a ferroelectric memory. When the electric field is even more negative than E_c, the domains start to align in the opposite direction until the polarization reaches saturation in the reverse direction. This is known as polarization reversal. To bring the negative polarization back to zero, a positive electric field is needed. In this way, the cycling of electric field results in a

hysteresis loop in the plot of polarization versus electric field; it is the characteristic hysteresis loop that indicates ferroelectricity.

A typical ferroelectric material is barium titanate $BaTiO_3$. It is presented as an example to illustrate some properties of ferroelectrics. As shown in Figure 2.6, $BaTiO_3$ has a perovskite crystal structure, in two different ways. Figure 1.8*a* shows the Ti^{4+} ion at the center of a cubic unit cell, with oxygen ions at the faces and Ba ions at the corners. Figure 1.8*b* puts the Ba ion at the cube center, and Ti ions, octahedrally coordinated by oxygen ions, at the corners. When a field is applied below the Curie temperature, the anions all move in one direction, and the cations in the other, destroying the cubic symmetric, and leaving the unit cell with a net dipole moment. When the field is reduced to zero the ferroelectric is left with a remnant polarization. This can only be removed by applying a negative coercive field E_c. At the high temperature $BaTiO_3$ presents a paraelectric phase there is no spontaneous polarization. Below the transition temperature (T_c =120ºC), spontaneous polarization occurs, and the crystal structure becomes slightly elongated, that is, tetragonal. $BaTiO_3$ exhibit the piezoelectric effect in the ferroelectric phase, while in the paraelectric, it is non-piezoelectric and exhibit only the electrostrictive effect. With decreasing temperature from room temperature, however, barium titanate transforms three ferroelectric phase transitions, a low temperature has phase rhombohedral and orthorhombic, with high temperature has phase tetragonal from cubic. [11]

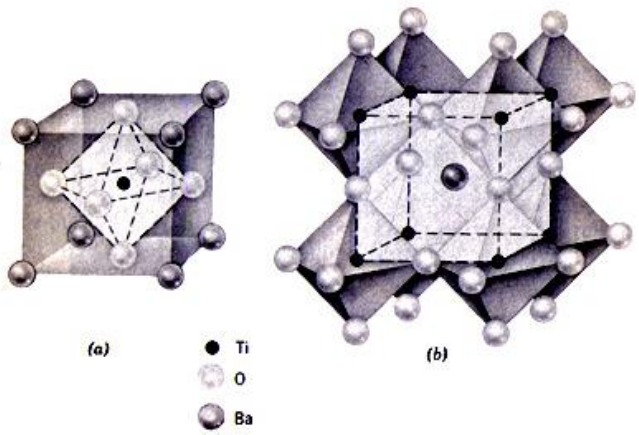

Figure 2. 6 (a) *Perovskite structure of $BaTiO_3$. (b) Ion position of $BaTiO_3$ above the Curie temperature.* [10]

Ferroelectric materials, especially polycrystalline ceramics, are very promising for variety of applications such as high permittivity capacitors, ferroelectric memories, pyroelectric sensors, piezoelectric transducers, electro-optic devices and PTC thermistors.

2.3 Crystal structure and ferrimagnetic properties of $CoFe_2O_4$

Cobalt ferrite $CoFe_2O_4$ has a spinel crystal structure with AB_2X_4 formula. Where A is a divalent cation, B is and a trivalent cation and X is a divalent anion in the stoichiometric formula of AB_2X_4 including oxides, sulfides, selenides and tellurides [13]. The cations A and B can occupy two different sites in a spinel structure, i.e octahedral (O_h) and tetrahedral (T_d) sites within the fcc oxygen sub-lattices. The occupations of metals at O_h and T_d sites have an important effect on the properties as spinel, such as color, diffusivity, magnetic behavior, conductivity and catalytic activity [14], [15]. The actual distribution of cations A and B in spinels is influenced by the heat treatment process and chemical environment [13]. The cation

distribution can be distinctly characterized by the so-called degree of inversion x, which is defined as the fraction of the divalent metal cations in octahedral sites as follows:

$$(Co_{1-x}Fe_x)_{Tet}[Co_xFe_{2-x}]_{Oct}O_4 \qquad \textbf{(4)}$$

In normal spinels (x=0), the tetrahedral and octahedral sites are occupied by divalent and trivalent cations, respectively, while in the inverse spinels (x =1) all the divalent cations occupy the octahedral sites and trivalent cations occupy tetrahedral and octahedral sites evenly. When it is a partial inverse structure, the spinel is called disordered since the di-and trivalent cations may be distributed at both tetrahedral and octahedral sites. The numbers of trivalent and divalent ions are required to remain at 2: 1 in a stable AB_2O_4. Typical normal spinels at room temperature are $MgAl_2O_4$, $FeAl_2O_4$, $ZnAl_2O_4$ and $FeCr_2O_4$ while Fe_3O_4, $MgFe_2O_4$ and $NiFe_2O_4$ are typical inverse spinels [16]. The spinel oxides can accommodate various cations, some of which may have multiple oxidation states, distributing at the tetrahedral and octahedral sites in different ways. Co ions of both 2^+ and 3^+ oxidation state can co-exist in the $CoFe_2O_4$ ferrites and so do Fe ions in the Fe_3O_4 ferrites.

The conventional unit cell of the spinel structure contains eight formula units as shown in figure 2.7, and it belongs to the *Fd3m* space group (2 2 7). Cations occupy 8a and 16d special Wyckoff positions of T_d and O_h symmetries at (0, 0, 0) and (5/8, 5/8, 5/8), respectively, whereas oxygen ions occupy the 32e positions at (u, u, u) [17]. Here *u* is the positional parameter of oxygen. It should be noted that the spinel is a relatively open structure since cations only occupy around 33% volume of the octahedral and tetrahedral voids [18].

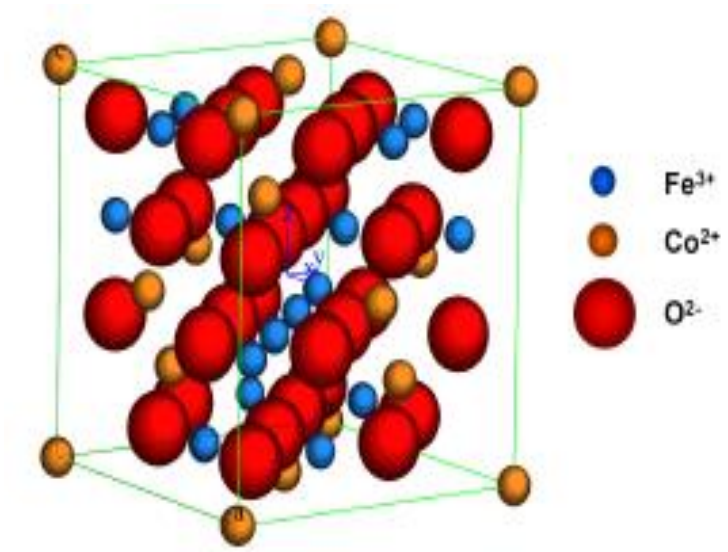

Figure 2. 7 *The cubic cell of spinel structure. The tetrahedral and octahedral cation sites are denoted by blue and golden spheres, respectively, while the oxygen atoms are represented by the big red spheres.* [10]

The spinel cobalt ferrite ($CoFe_2O_4$) has a wide range of applications including electronic devices, ferrofluids, magnetic delivery microwave devices and high density information storage due to its wealth of magnetic and electronic properties, such as high magnetostriction and high rate of change of strain with magnetic field, cubic magnetocrystalline anisotropy, high coercivity, moderate saturation magnetization, high Curie temperature, photomagnetism, high chemical stability and good electrical insulation [19].

2.4 Crystal structure and electrical properties of $Bi_4Ti_3O_{12}$

Bismuth titanate $Bi_4Ti_3O_{12}$ is layered perovskite structured with a general formula $(Bi_2O_2)^{2+}(A_{n-1}B_nO_{3n+1})^{2-}$ where A is a mono, di or trivalent large cation (or a mixture of them) like $Na^+, K^+, Ca^{2+}, Ba^{2+}, Sr^{2+}, Pb^{2+}, Bi^{3+}$. B is a tri, tetra, penta or hexavalent small cation with

high electric charge (or a mixture of them) like $Fe^{3+}, Ti^{4+}, Nb^{5+}, Ta^{5+}, Mo^{6+}, W^{6+}$, and n is the number of perovskite layers [2].

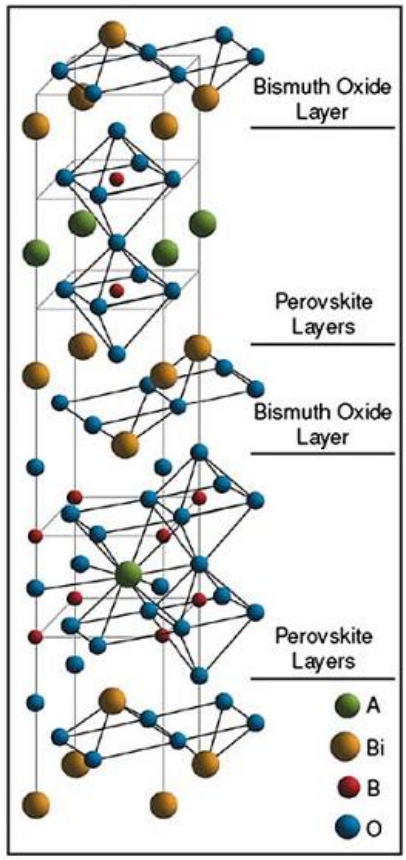

Figure 2. 8 *Structure of a layered perovskite ferroelectric with n = 2* [20]

The crystal structure of $Bi_4Ti_3O_{12}$ consist of $(A_{n-1}B_nO_{3n+1})^{2-}$ sheets along the *c*-axis between two bismuth oxide $(Bi_2O_2)^{2+}$, as shown in Figure 2.8 [21], if *n* is even, the group of layered perovskite located between the bismuth oxide layers have a center position *A* and has a plane symmetry element perpendicular to the *c* axis octahedral separates, if *n* is odd, the center is in position *B* and the plane symmetry divides the octahedral. The plane parallel to the layers of bismuth oxide *a-b* plane is defined as the primitive cell, so that the stack of tissue layers along

the *c* axis. At room temperature the symmetry of $Bi_4Ti_3O_{12}$ is monoclinic structure with the space group $B1a1$, while it can be considered as orthorhombic structure with the lattice constant of the *c*-axis $(c = 3.2843nm)$, which is considerably larger than that of the other two axis $(a = 0.5445nm, b = 0.5411nm)$ [22]. This structure is responsible for the anisotropy having its physical properties. The Curie temperature of $Bi_4Ti_3O_{12}$ is 675 ºC, which make it a suitable candidate for high-temperature piezoelectric devices [23].

Bismuth titanate $Bi_4Ti_3O_{12}$ with a bismuth layer structure exhibits good ferroelectric properties and fatigue durability [24], [25]. Due to the two-dimensional layer structure, as shown in Figure 2.9, the electrical anisotropy is high: continuous B-O-B-O chains, which are necessary for ferroelectric behavior, are only present along the a- or b-axis, but not in the c-axis. Ferroelectricity of the Aurivillius phases is mainly caused by shift of the B cations outside the center of the oxygen octahedron along the a-axis and by deformation (tilt, rotation and shift) of the oxygen octahedron. Hence, for even *n* there is no polarization along the c-axis and for odd *n* there is only small polarization along the *c*-axis [26]. $Bi_4Ti_3O_{12}$ has a spontaneous polarization in the *a*-*c* plane and exhibit two independently reversible components along the *c* and *a* axis [7].

By substituting different cations a large diversity of compounds can be realized, which allows better ferroelectric properties, such as large polarization and coercive field (P_r, E_c). However many factors may influence the ferroelectric properties in these compounds, namely:

i. Structure, particularly if the structure is a perovskite or an Aurivillius phase as well as the value of *m* [27], [28]

ii. Chemical composition [3], [29]–[31]

iii. Orientation [29], [32]–[35]

iv. Defect density [7], [32]

v. Domain structure [36]

vi. Substrate type [37]–[40]

vii. Film thickness [41]

Thus $Bi_4Ti_3O_{12}$ is a potential candidate for many applications, especially for nonvolatile memories, due to its relatively low coercive field, relatively small dielectric constant and high Curie temperature.

2.5 Magneto-electric coupling

The term multiferroism has been attributed to describe materials where ferroelectricity, ferroelasticity and ferromagnetism occur in the same phase. This means that they have a spontaneous magnetization, which can be reoriented by an applied magnetic field, a spontaneous polarization which can be reoriented by an applied electric field, and a spontaneous deformation, which can be oriented by an applied stress. The coupling between ferromagnetism and ferroelectricity results in magnetoelectricity [42]. Figure 2.9 shows schematically the multiferroic behavior. However, this coupling proved to be a difficult problem, as this order parameters turn out to be mutually exclusive. Furthermore, simultaneous presence does not guarantee strong coupling, as microscopic mechanisms of ferroelectricity and magnetism are quite different.

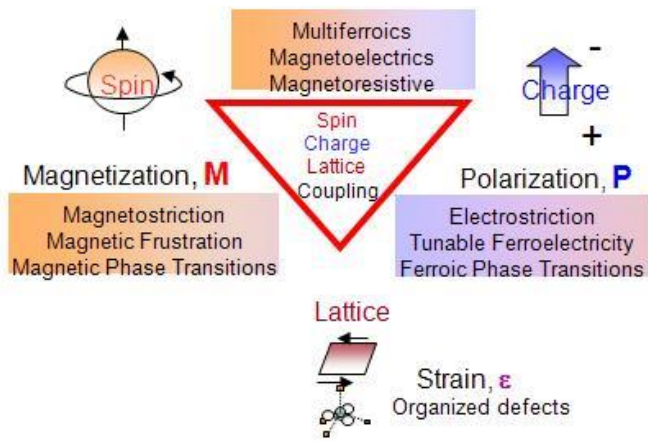

Figure 2. 9 *Relationship between multiferroic, magnetoelectrics and magnetoresistive materials*. [43]

A requirement for the existence of ferroelectricity is a structural distortion from the high symmetry phase that removes the center of symmetry and allows an electric polarization. There are 31 point groups that allow a spontaneous electric polarization and 31 that allow a spontaneous magnetic polarization [44]. Thirteen point groups (1, 2, 2`, *m*, *m*`, 3, 3*m*`, 4, 4*m*`*m*`, *m*`*m*2`, *m*`*m*`2`, 6, and 6*m*`*m*`) are found in both sets, allowing both properties to exist in the same phase. Besides these groups, many candidate materials (that are not in fact ferroelectric and ferromagnetic) exist in one of the allowed symmetries.

The magneto-electric effect in a crystal is traditionally described in Landau theory by writing the free energy *F* of the system in terms of an applied magnetic field *H* and an applied electric field *E*. Using Einstein summation convention *F* can be written as

$$-F(E,H)=\frac{1}{2}\varepsilon_0\varepsilon_{ij}E_iE_j+\frac{1}{2}\mu_0\mu_{ij}H_iH_j+\alpha_{ij}E_iH_j+\frac{\beta_{ijk}}{2}E_iH_jH_k+\frac{\gamma_{ijk}}{2}H_iE_jE_k+.... \quad \textbf{(5)}$$

The first term on the right hand side describes the contribution resulting from the electrical response to an electric field, where ε_{ij} *(T)* is relative permittivity. The second term is the magnetic equivalent of the first term, where μ_{ij} *(T)* is relative permeability, the third term

describes linear magneto-electric coupling via α_{ij} *(T)*. Other terms represent higher-order magneto-electric coupling coefficients. The magneto-electric effect can be established in the forms P_i (H_j) or $M_i(E_j)$ by differentiating F. One obtains:

$$P_i(H_j) = \alpha_{ij} H_j \frac{\beta_{ijk}}{2} H_j H_k + ...$$
$$M_i(E_j) = \alpha_{ij} E_j \frac{\gamma_{ijk}}{2} E_j E_k + ...$$
(6)

Term α_{ij} is designated as the linear magneto-electric effect and corresponds to the induction of polarization by a magnetic field or a magnetization by an electric field. Materials exhibiting magneto-electric coupling are Cr_2O_3, $BiMnO_3$, and $BiFeO_3$. Unfortunately, the magneto-electric coupling is usually too small to be practically applicable as term α_{ij} is limited by the relation:

$$\alpha_{ij}^2 \leq \varepsilon_{ii} \mu_{jj} \quad \textbf{(7)}$$

Early work on multiferroic properties were released from the 1960s, the first ferromagnetic ferroelectric material to be discovered was nickel iodine boracite, $Ni_3B_7O_{13}I$, where ferroelectricity and weak ferromagnetism have been found [45].

Other ferromagnetic ferroelectrics are metal oxide has been the focus of much study because of the wide range of structures and properties present in these materials, the which most commonly is using are the ternary oxides structures, include the ilmentite structure (i.e., $FeTiO_3$, $LaMnO_3$, $MnTiO_3$, $YMnO_3$, $BiMnO_3$ and $LiNbO_3$) [46] [47], Spinel structure (i.e., $MgAl_2O_4$, $CoFe_2O_4$ and $LiTi_2O_4$), Perovskite structure (i.e., $CaTiO_3$, $SrRuO_3$, $SrTiO_3$, $KTaO_3$**,** $BaTiO_3$, and $BiFeO_3$) Figure 1.10 (c). One of the famous multiferroic perovskite structure is $BiFeO_3$ due to its possible applications, bismuth ferrite shows ferroelectric ordering with high Curie temperature (T_c = 1103 K) and antiferromagnetic ordering with high Neel temperature (T_N = 634K) [9]. And

perovskite-derived structures such as the Ruddlesden-Popper series Figure 1.10 (d), and other layered-perovskite structure Figure 2.11 (e) [1].

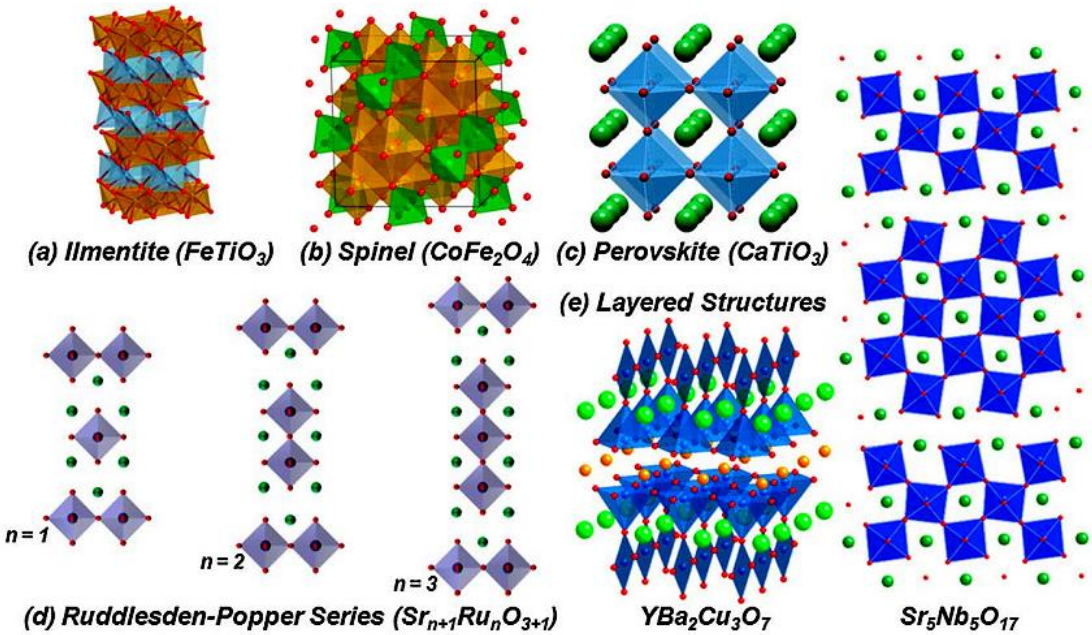

Figure 2. 10 *Common ternary oxide crystal structures including (a) ilmentite, (b) spinel, (c) perovskite, (d) Ruddlesden–Popper series and (e) layered perovskites. [1]*

For chemical coupling between ferromagnetic and ferroelectric in these oxide is used the replacement of some of the d^o B cations in perovskite oxides by magnetic d^n cations. Some common small cations found in ferroelectric perovskite oxide are: Ti^{4+} 74.5 pm; Nb^{5+} 78 pm and Zr^{4+} 86 pm. Some representative d^n cations that are found as the small cations magnetic oxides include Mn^{3+} (d^4) 78.5 pm, Ti^{3+} (d^1) 81 pm, and V^{4+} (d^1) 72 pm. Therefore, typical B-site cations with *d* electron occupation do not have systematically larger radii than typical d^0 b-site cations [43]. Following this principle the first synthetic ferromagnetic ferroelectric material was, (1 – x)Pb $(Fe_{2/3}W_{1/3})O_3$ –xPb$(Mg_{1/2}W_{1/2})O_3$ [48], here the Mg^{2+} and W^{6+} ions are diamagnetic and

cause the ferroelectricity, and the formally d^5 Fe^{3+} ion is responsible for the magnetic ordering. Other examples the replacements B-site are: $Pb_2(CoW)O_6$ which is ferroelectric and ferromagnetic, [49]. $Pb_2(FeTa)O_6$ which is ferroelectric and anti-ferromagnetism [50]. $SrBi_2Ta_2O_9$ would be ferromagnetic as well as ferroelectric [51]. However, dilution of the magnetic ions in these materials has rather a low Curie or Néel Temperature. Other compound is $(Bi_{4-x}Gd_x)(Ti_{3-y}Fe_y)O_{12}$ ferroelectric and weak ferromagnetism is observed [52]. A large amount of research has been focused on substitution of d^o B cations in perovskite oxides and magnetic d^n cations for better coupling ferroelectric and ferromagnetic.

However recent studies have focused in the fabrication of thin film multilayers. Such films consisting of alternating layers of the ferroelectric and ferro or ferrimagnetic phase. For the ferroelectric phase is used oxides perovskite such as $BaTiO_3$ and $BiFeO_3$ and for ferro/ferrimagnetic phase is used spinel structure such as $MgAl_2O_4$ or $CoFe_2O_4$. Recent work shows alternating layers of $BaTiO_3/CoFe_2O_4$ [53] and $Bi_{0.8}La_{0.2}Ti_3O_{12}/CoFe_2O_4$ [54] multilayer thin films deposited by pulsar laser deposition (PLD).

Tri-layered film were presented using perovskite structure with cations substitute for earth rare, such as $Bi_{3.25}La_{0.75}Ti_3O_{12}/BiFeO_3/$ $Bi_{3.25}La_{0.75}Ti_3O_{12}$ deposited by chemical solution deposition (CSD) [55]. Also $(Bi_{0.9}La_{0.1})FeO_3/CoFe_2O_4/Bi_{0.9}La_{0.1})FeO_3$ deposited by rf sputtering [56].

Double-layers thin films are presented, used perovskite structures layers $BiFeO_3/Bi_4Ti_3O_4$ this thin films were fabricated by chemical solution deposition [57]. Multiferroic $BiFeO_3/CoFe_2O_4$ bi-layered films deposited by spin coating technique on the $LaNiO_3$ substrate [58]. Two set of layers were deposited, $1Bi_{3.5}Nd_{0.5}Ti_3O_{12}/1CoFe_2O_4$ and

$3Bi_{3.5}Nd_{0.5}Ti_3O_{12}/1CoFe_2O_4$ [5] and bilayer films $Bi_{3.15}Nd_{0.85}Ti_3O_{12}/CoFe_2O_4$ [8] deposited by spin coating.

Following this line of research we have worked in multilayer thin films, alternating layers of the ferroelectric phase, i.e. perovskite $Bi_4Ti_3O_{12}$ with partial substituting by trivalent lanthanide ions other than La^{3+}, such as Sm^{3+}, and Nd^{3+}. The ionic radii of some of these elements are Bi (0.117 nm), La (0.116 nm), Sm (0.108 nm) and Nd (0.111 nm). And the ferrimagnetic phase, i.e. spinel structure $CoFe_2O_4$.

III. EXPERIMENTAL

3.1 Materials and Synthesis of solutions

The chemical solution route was used these materials for the synthesis:

- Bismuth nitrate (III) pentahydrate 98% [$Bi(NO_3)_3.5H_2O$]
- Lanthanum nitrate (III) hexahydrate 99.999% [$La(N_3O_9).6H_2O$]
- Samarium nitrate (III) hexahydrate 99.99% [$Sm(NO_3)_3.6H_2O$]
- Titanium isopropoxide 99.999% [$C_{12}H_{28}O_4Ti$]

Were used as precursors for Bi, La, Sm, Nd and Ti, respectively, 2-Methoxyethanol was used as a solvent. To achieve specific compositions in the chemical solution of the $Bi_{4-x}M_xTi_3O_{12}$ (M = La and Sm) and x = 0.6 the following formula was used:

$$Bi = (4-x)\left(\frac{00.8molBi}{1molSol}\right)\left(40\times10^{-3}L\right)\left(\frac{1molBi_{nitrate}}{1molBi}\right)\left(\frac{F.W.Bi_{nitrate}}{1LSol}\right)\left(\frac{100gr}{98gr}\right) \quad \textbf{(8)}$$

$$M = (x)\left(\frac{00.8molM}{1molSol}\right)\left(40\times10^{-3}L\right)\left(\frac{1molM_{nitrate}}{1molM}\right)\left(\frac{F.W.M_{nitrate}}{1LSol}\right)\left(\frac{100gr}{gr}\right) \quad \textbf{(9)}$$

$$Ti = (3)\left(\frac{00.8molTi}{1molSol}\right)\left(40\times10^{-3}L\right)\left(\frac{1molTi_{isop}}{1molTi}\right)\left(\frac{F.W.Ti_{isop}}{1LSol}\right)\left(\frac{100gr}{99.999gr}\right) \quad \textbf{(10)}$$

To prepare $Bi_{4-x}M_xTi_3O_{12}$ precursor solution, bismuth nitrate (10 mol. % excess) and M (M = La and Sm) were dissolved in 20ml of 2-Methoxyethanol [$C_3H_8O_2$] solvent and stirred at

room temperature for 1 hours. Titanium isopropoxide was dissolved in 20 ml of 2-Methoxyethanol and stirred for 30 min and mixed with $Bi_{3.4}La_{0.6}$ solution and stirred finally for 12 hours to achieve homogeneous and transparent solution, see Figure 3.1. The total volume of this solution was 40 ml with a final concentration of 0.08 molar.

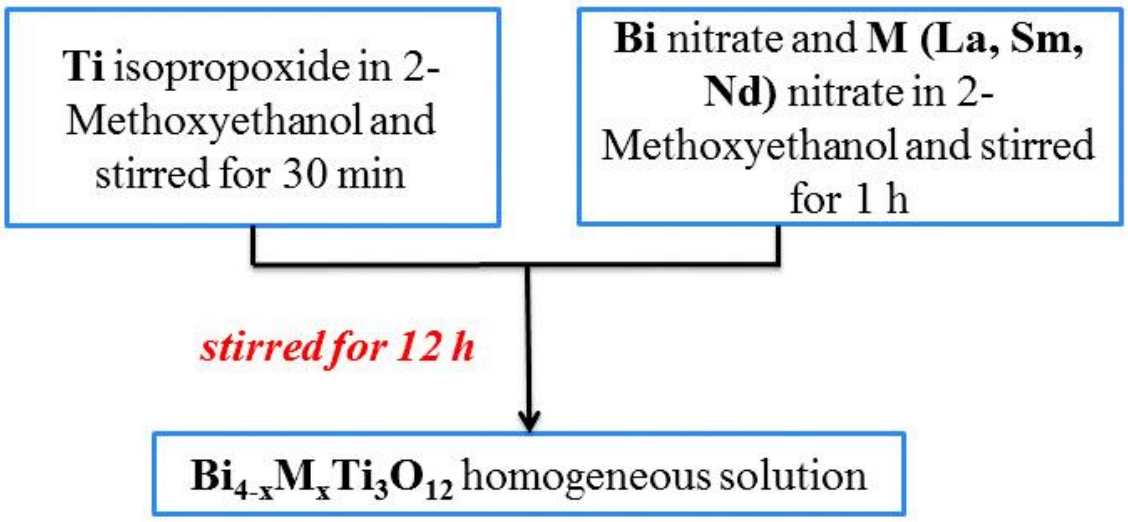

Figure 3. 1 *The chemical solution routes for* $Bi_{4-x}M_xTi_3O_{12}$

For chemical route solution $CoFe_2O_4$ was used these materials:

- Cobalt (II) nitrate hexahydrate 99.999% [$CoN_2O_6.6H_2O$]
- Iron (III) nitrate nanohydrate 99.99% [$FeN_3O_9.9H_2O$]

Cobalt (II) nitrate hexahydrate and iron (III) nitrate nanohydrate were used as precursors for Co and Fe, respectively; 2-Methoxyethanol was used as a solvent. The same formula was used:

$$Co = \left(\frac{00.8molCo}{1molSol}\right)\left(40\times10^{-3}L\right)\left(\frac{1molCo_{nitrate}}{1molCo}\right)\left(\frac{F.W.Co_{nitrate}}{1LSol}\right)\left(\frac{100gr}{99.999gr}\right) \quad \textbf{(11)}$$

$$Fe = (2)\left(\frac{00.8molFe}{1molSol}\right)\left(40\times10^{-3}L\right)\left(\frac{1molFe_{nitrate}}{1molBi}\right)\left(\frac{F.W.Fe_{nitrate}}{1LSol}\right)\left(\frac{100gr}{99.99gr}\right) \quad \textbf{(12)}$$

$CoFe_2$ were dissolved is 40ml of 2-Methoxyethanol solvent and stirred for 12 hours at room temperature to achieve homogeneous solution, see Figure 3.2. The total volume of this solution was 40 ml with a final concentration of 0.2 molar.

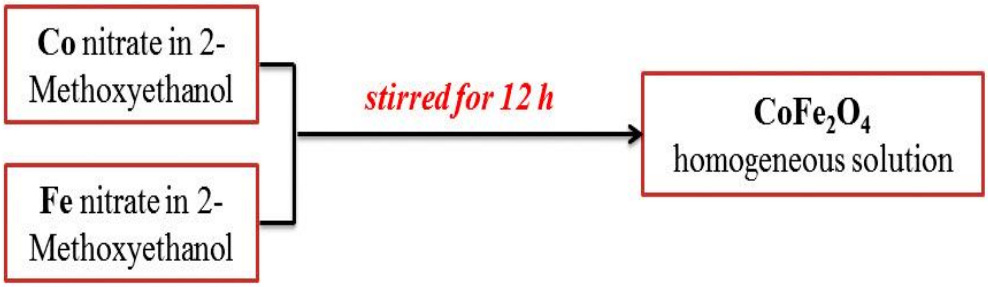

Figure 3. 2 *The chemical solution routes for $CoFe_2O_4$*

The solution were deposited onto Platinum ($Pt/Ti/SiO_2/Si$) pieces (~ 0.8 cm x 0.8 cm), the substrate were cleaned with distilled water and acetone ACS 99.5% (CH_3COCH_3), and dried in a hotplate at 400ºC for 10 min, the multilayer thin films were deposited by spin coating technique.

3.2 Spin Coating Description

Consists in which a drop of the fluid is deposited onto the substrate surface, a high speed spin step to thin the fluid, and a drying step to eliminate excess solvents from the resulting film. There two common methods of deposited are: static deposited, and dynamic deposited.

Static deposited is simply depositing a drop of fluid on or near the center of the substrate. The amount of drops dispensed can range depending on the viscosity of the fluid and the size of

the substrate to be coated. Higher viscosity and or larger substrates typically require a larger puddle to ensure full coverage of the substrate during the high speed spin step.

Dynamic deposited is the process of dispensing while the substrate is turning at low speed. A speed of about 500 - 1000 rpm is commonly used during this step of the process. This serves to spread the fluid over the substrate and can result in less waste of material since it is usually not necessary to deposit as much to wet the entire surface of the substrate. This is a particularly advantageous method, because can eliminate voids in the surface in the films.

After the deposited step it is common to accelerate to a relatively high speed to thin the fluid to near its final desired thickness. Typical spin speeds for this step range from 1500-6000 rpm, again depending on the properties of the fluid as well as the substrate. This step can take from seconds to several minutes. The combination of spin speed and time selected for this step will generally define the final film thickness; in general, higher spin speeds and longer spin times create thinner films, see Figure 3.3.

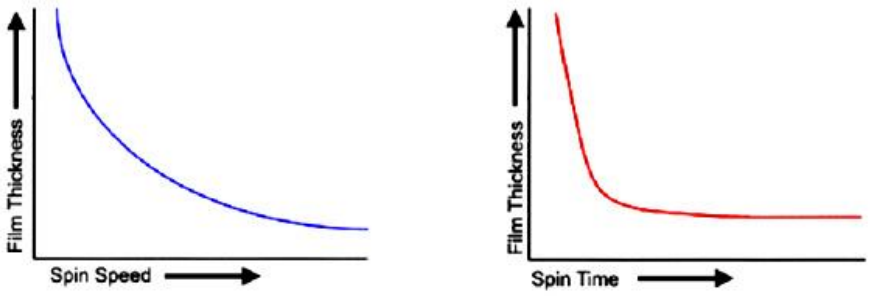

Figure 3. 3 *Speed and Time for define the final film thickness*

A separate drying step each of the layers deposited after the high speed spin step to further dry the film. The drying is carried out in a hot plate at 400ºC for 5 minutes. After each

step of drying, be repeat the spin coating process to obtain the desired number of layers. In Figure 3.4 we can observe this process graphically.

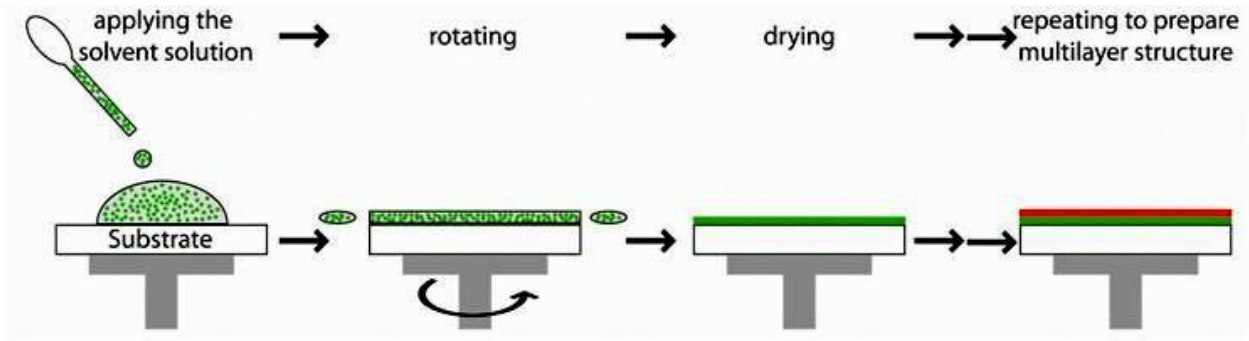

Figure 3. 4 *Spin coating process for multilayer thin films*

Finally, we get multilayer thin films its geometry consisting of alternating layers of the ferroelectric phase (perovskite $Bi_{3.4}M_{0.6}Ti_3O_{12}$ with M=La and Sm) and the ferrimagnetic phase (spinel $CoFe_2O_4$) as shows Figure 3.5. After all the layers deposited these films were annealing in a furnace at 750 for 20 minutes, under oxygen atmosphere.

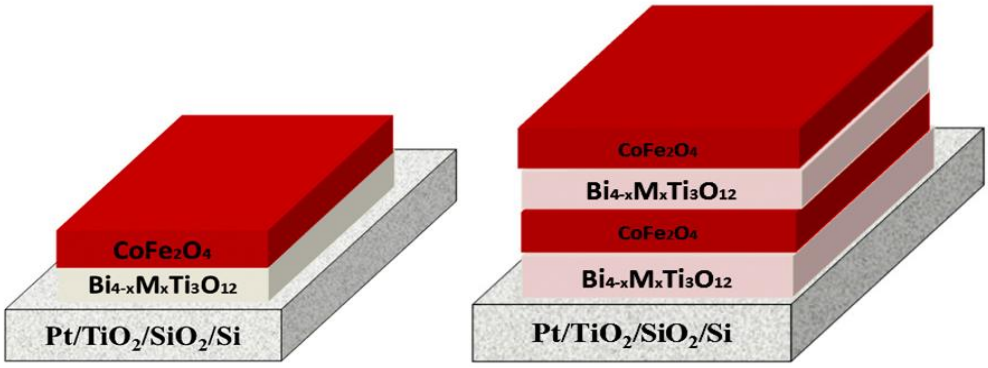

Figure 3. 5 *Bi-layer and four-layer thin films, deposited on Pt ($Pt/TiO_2/SiO_2/Si$) substrate.*

3.3 CHARACTERIZATION OF THE THIN FILMS

Structural analysis of the thin films was carried out in Rigaku Ultima III x-ray diffractometer using the Cu Kα radiation (0.15405 nm). The magnetic properties were characterized using a Lake Shore's new 7400 series Vibrating Sample Magnetometer (VSM). The thicknesses of the films were measured by profilometer. Electrical measurements were performed using a Pt-multilayer thin film-Pt capacitor configuration. These capacitors, were fabricated depositing Pt top electrodes on the surface of the multilayer thin film with an area of 3.14×10^{-4} cm^2 utilizing the masking technique by dc sputtering. The ferroelectric hysteresis loops were measured with a RT 6000 HVS probe ferroelectric tester (Radiant technology). The dielectric constant, loss tag δ, and frequency were measured with an impedance analyzer HP4294a (in the range from -10V to 10V and 1 KHz to 1MHz) respectively. The leakage current was measured with a Keithley 2401. Scanning Electron Microscopy (SEM) technique was used to observe the morphology of the films and microstructures defects. All these measurements were carried out at room temperature.

3.3.1 X-ray diffraction (XRD)

X-ray diffraction (XRD) is one of the most important non-destructive characterization technique used to analyze the structural properties of matter. The XRD is a rapid analytical technique primarily used for phase identification of a crystalline material and can provide information on unit cell dimensions, the lattice parameters, the strain and the grain size. X-ray diffractometers consist of three basic elements: an x-ray tube, a sample holder, and an x-ray

detector, in a cathode ray tube by heating a filament to produce electrons, accelerating the electrons toward a target by applying a voltage, and bombarding the target material with electrons. When electrons have sufficient energy to dislodge inner shell electrons of the target material, characteristic X-ray spectra are produced. Copper is the most common target material for single-crystal diffraction, with Cu Kα (radiation = 0.15405 nm). These x-rays are collimated and directed onto the sample. As the sample and detector are rotated, the intensity of the reflected x-rays is recorded.

When the geometry of the incident x-rays impinging the sample satisfies the Bragg Equation, constructive interference occurs and an intensity peak occurs. A detector records and processes this x-ray signal and converts the signal to a count rate which is then output to a device. The geometry of an x-ray diffractometer is such that the sample rotates in the path of the collimated x-ray beam at an angle Θ while the X-ray detector is mounted on an arm to collect the diffracted x-rays and rotates at an angle of 2Θ [59].

3.3.2 Vibrating Sample Magnetometer (VSM)

Vibrating Sample Magnetometer (VSM) is an instrument based on the principle of electromagnetic induction. The basic measurement is accomplished by oscillating the sample near a detection (pick-up) coil and synchronously detecting the voltage induced. By using a compact gradiometer pickup coil configuration, relatively large oscillation amplitude (1-3 mm peak) and a frequency of 40 Hz, the system is able to resolve magnetization changes of less than 10^{-6} emu at a data rate of 1 Hz.

VSM consists primarily of a linear motor transport (head) for vibrating the sample, a coil set puck for detection, electronics for driving the linear motor transport and detecting the response from the pickup coils, and a software application for automation and control. The sample is attached to the end of a sample rod that is driven sinusoidal. The center of oscillation is positioned at the vertical center of a gradiometer pickup coil. The precise position and amplitude of oscillation is controlled from the VSM motor module using an optical linear encoder signal read back from the VSM linear motor transport. The voltage induced in the pickup coil is amplified and lock in detected in the VSM detection module. The VSM detection module uses the position encoder signal as a reference for the synchronous detection. This encoder signal is obtained from the VSM motor module, which interprets the raw encoder signals from the VSM linear motor transport. VSM is one of the most commonly used magnetometers for the characterization of magnetic materials in both the research laboratory and the production factory [60].

3.3.3 Dc Sputtering

Dc Sputtering is a technique used for depositing materials onto a substrate, by ejecting atoms from such materials and condensing the ejected atoms onto a substrate in a high vacuum environment.

The basic process is a follows: A target or source of the material desired to be deposited, is bombarded with energetic ions, typically inert gas ions such as Argon (Ar^+). The forceful collision of these ions onto the target ejects target atoms into the space. These ejected atoms then travel some distance until they reach the substrate and start to condense into a film. As more and

more atoms coalesce on the substrate, they begin to bind to each other at the molecular level, forming a tightly bound atomic layer. One or more layers of such atoms can be created will depending on the sputtering time, allowing for production of precise layered thin-film structures. Figure 3.8 shows the dc sputtering system, where Argon is ionized by a strong potential difference, and these ions are accelerated to a target. After impact, target atoms are released and travel to the substrate, where they form layers of atoms in the thin-film.

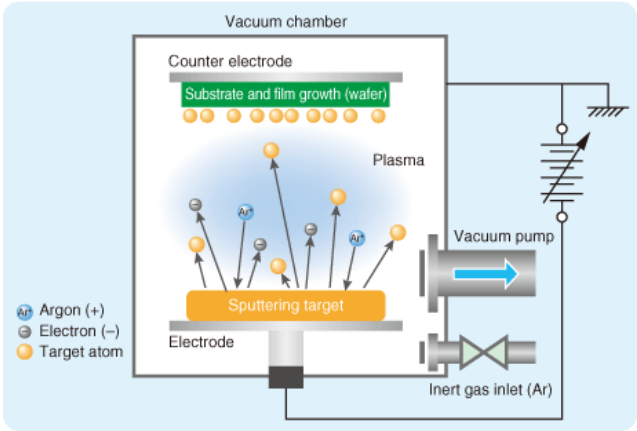

Figure 3. 6 *Dc Sputtering systems*

Though the basic idea of operation is seemingly simple, the actual mechanism is quite complex. Electrically neutral Argon atoms are introduced into a vacuum chamber at a pressure of 1 to 10mTorr. A DC voltage is placed between the target and substrate which ionizes Argon atoms and crate plasma, hot gas-like phase consisting of ions and electrons, in the chamber. This plasma is also known as a glow discharge due to the light emitted. These Argon ions are now charged and are accelerated to the anode target. Their collision with the target ejects target atoms, which travel to the substrate and eventually settle. Electrons released during Argon ionization are accelerated to the anode substrate, subsequently colliding with additional Argon atoms, creating more ions and free electrons in the process.

3.3.4 Ferroelectric Tester

Hysteresis loop, polarization versus electric field (P-E) was measured using the RT 6514 HVS ferroelectric tester (Radiant technology). The most used method of hysteresis loop measurement is based on a paper by Sawyer and Tower [61]. A schematic of the experimental setup is shown in Figure 3.9, in which *C* is the capacitance of the ferroelectric thin films and C_0 is the standard capacitor. The voltage across *C* should be sufficiently large to render saturation in polarization, so V_0 should be proportional to the polarization charge, $V_0 = AP / C_0$ where *A* is the area of the specimen. *V* is the applied voltage, which is usually an *AC* signal voltage of low frequencies. Thus, the applied field across the specimen is $E = V_c / d = (V - V_0) / d$, where *d* is the thickness of thin films.

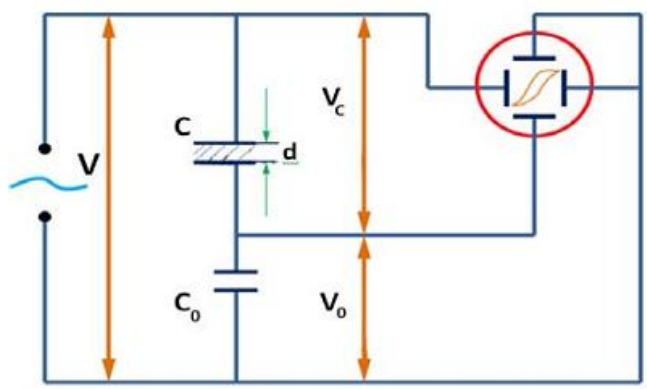

Figure 3. 7 *The Sawyer Tower method for the measurement of the polarization-electric field (P-E) characteristics* [61].

3.3.5 Scanning Electron Microscopy (SEM)

The scanning electron microscope (SEM) uses a focused beam of high-energy electrons to generate a variety of signals at the surface of solid specimens. The signals that derive from

electron-sample interactions reveal information about the sample including external morphology, chemical composition, and crystalline structure and orientation of materials making up the sample. In most applications, data are collected over a selected area of the surface of the sample, and a 2-dimensional image is generated that displays spatial variations in these properties [62].

The fundamental principle of Scanning Electron Microscopy is accelerated electrons in an SEM carry significant amounts of kinetic energy, and this energy is dissipated as a variety of signals produced by electron-sample interactions when the incident electrons are decelerated in the solid sample. These signals include secondary electrons (that produce SEM images), backscattered electrons (BSE), diffracted backscattered electrons (EBSD that are used to determine crystal structures and orientations of minerals), photons (characteristic X-rays that are used for elemental analysis and continuum X-rays), visible light (cathodoluminescence--CL), and heat.

Secondary electrons and backscattered electrons are commonly used for imaging samples: secondary electrons are most valuable for showing morphology and topography on samples and backscattered electrons are most valuable for illustrating contrasts in composition in multiphase samples (i.e. for rapid phase discrimination). SEM analysis is considered to be "non-destructive" that is, x-rays generated by electron interactions do not leading to volume loss of the sample [63].

IV. RESULT AND DISCUSSION

4.1 $CoFe_2O_4/Bi_{3.4}La_{0.6}Ti_3O_{12}/Pt$ Multilayers Structure

a. Structural Properties

$CoFe_2O_4/Bi_{3.4}La_{0.6}Ti_3O_{12}/Pt$ was characterized by x-ray diffraction (XRD) showing c-axis polycrystalline growth as observed in Figure 4.1. For comparison, the x-ray diffraction patterns of $CoFe_2O_4/Pt$ and $Bi_{3.4}La_{0.6}Ti_3O_{12}/Pt$ is included with $CoFe_2O_4/Bi_{3.4}La_{0.6}Ti_3O_{12}/Pt$ bilayer structure. The average thicknesses of the films were 190 nm for $CoFe_2O_4/Pt$, 250 nm for $Bi_{3.4}La_{0.6}Ti_3O_{12}/Pt$ and 550 nm for the bilayers film.

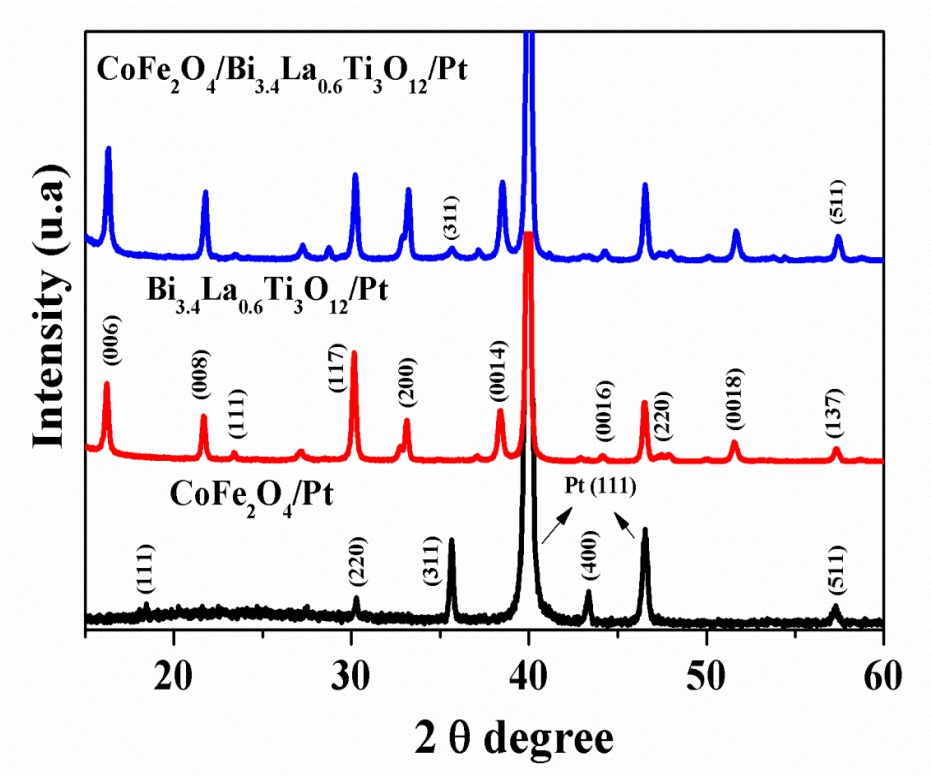

Figure 4. 1 *X-ray diffraction patterns of $CoFe_2O_4$, $Bi_{3.4}La_{0.6}Ti_3O_{12}$ films and $CoFe_2O_4$/ $Bi_{3.4}La_{0.6}Ti_3O_{12}$ bilayers structures on Pt substrate ($Pt/TiO_2/SiO_2/Si$).*

X-ray for $Bi_{3.4}La_{0.6}Ti_3O_{12}$ indicates that the La^{3+} ions are partially substituted on Bi^{3+} ion in $Bi_4Ti_3O_{12}$ perovskite structure. Diffraction pattern for $CoFe_2O_4$ and $Bi_{3.4}La_{0.6}Ti_3O_{12}$ films shows a preferential c-axis orientations, similar as reported earlier [64], [65].

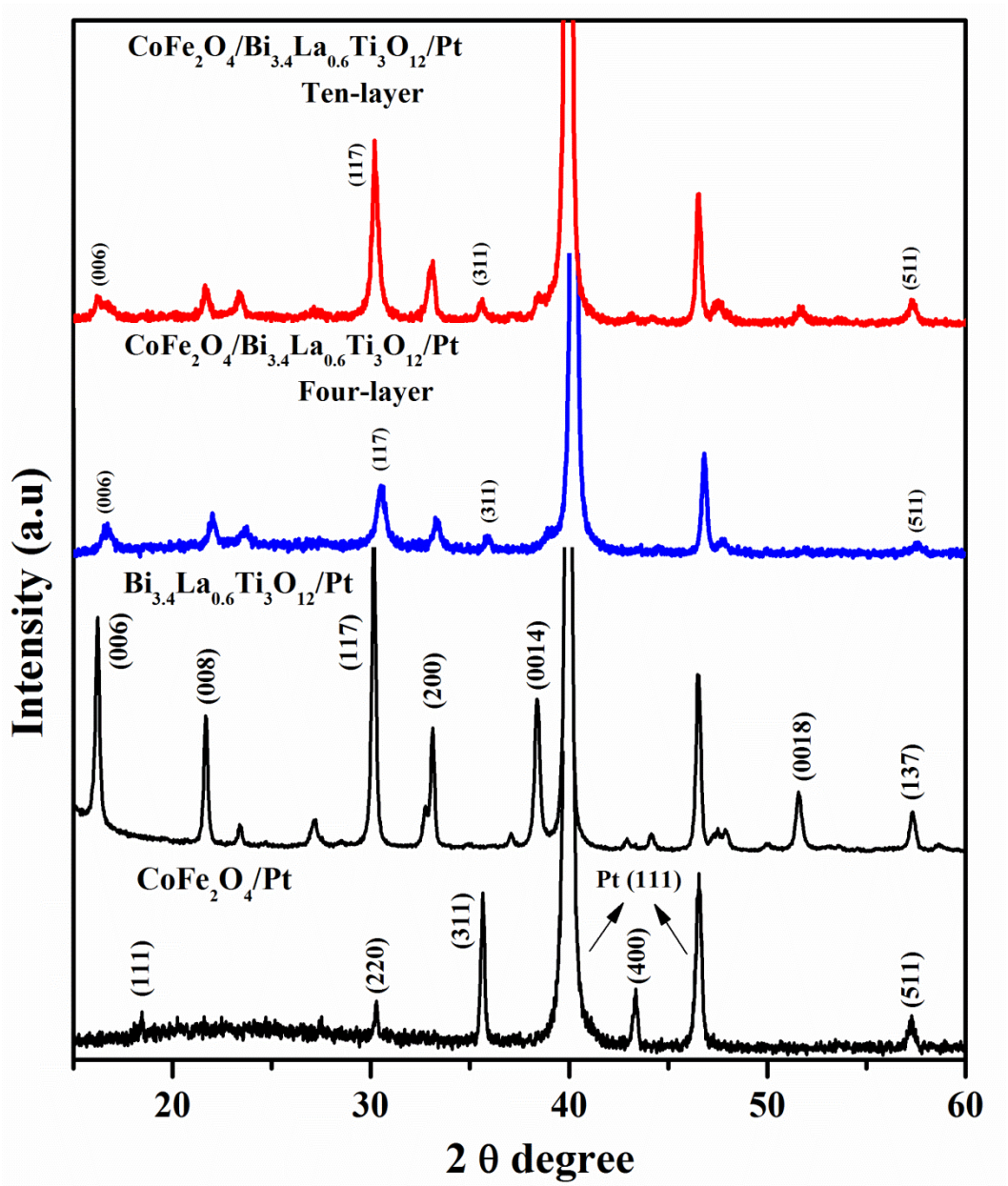

Figure 4. 2 *X-ray diffraction patterns of $CoFe_2O_4$, $Bi_{3.4}La_{0.6}Ti_3O_{12}$ films, $CoFe_2O_4/Bi_{3.4}La_{0.6}Ti_3O_{12}$ four-layer and $CoFe_2O_4/Bi_{3.4}La_{0.6}Ti_3O_{12}$ ten-layer structures*

The predominant x-ray diffraction peaks (006), (117), and (200) of $Bi_{3.4}La_{0.6}Ti_3O_{12}$ and (311) and (511) peaks of $CoFe_2O_4$ co-exist in the bilayer structure, indicating the bilayer system revealed the composite-like structure. To verify it we deposited four-layer and ten-layer structures.

$CoFe_2O_4/Bi_{3.4}La_{0.6}Ti_3O_{12}/Pt$ four-layer and ten-layer was characterized by x-ray diffraction as observed in Figure 4.2. We observe again (006), (117) peaks of $Bi_{3.4}La_{0.6}Ti_3O_{12}$ and (311) and (511) peaks of $CoFe_2O_4$ coexist in both multilayers. This confirms the composite-like structure. Therefore, x-ray diffraction establishes a composite–like structure of both multilayer structures in vertically aligned layers. The average films thicknesses were ~ 260 nm for four-layer and ~ 600 nm for ten layers.

Figure 4.3 shows the scanning electron microscopy (SEM) for $CoFe_2O_4/Bi_{3.4}La_{0.6}Ti_3O_{12}/Pt$ bilayer, four-layer, and ten-layer. Images shows polycrystalline films and the surfaces morphology did not present cracks or defects indicating of homogeneous topology of the films. Figure 4.3 (b) shows cross–sectional of $CoFe_2O_4/Bi_{3.4}La_{0.6}Ti_3O_{12}/Pt$ bilayer, structures of layers were formed with the thickness of the $Bi_{3.4}La_{0.6}Ti_3O_{12}$ higher than $CoFe_2O_4$ layers in the multilayers.

The average grain size is and 47 nm for $CoFe_2O_4/Bi_{3.4}La_{0.6}Ti_3O_{12}/Pt$ bilayer, 50 nm for four-layer, and 56 nm for ten-layer structures. These results are in agreement with the x-ray and calculated for Scherrer's equation. The cross-section shows polycrystalline film with varies thickness without segregation of impurity.

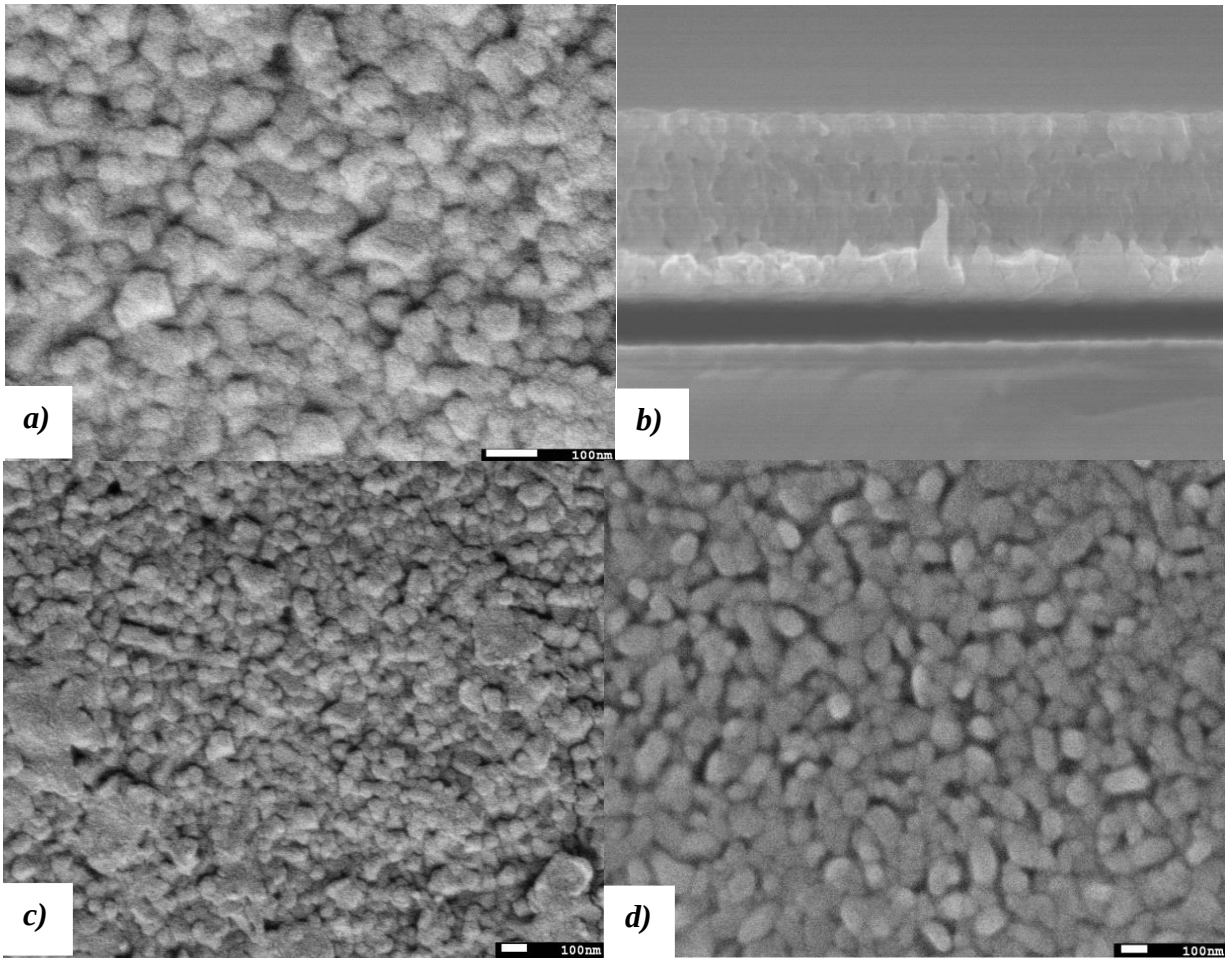

Figure 4. 3 *SEM micrograph showing surfaces morphology of (a) $CoFe_2O_4/Bi_{3.4}La_{0.6}Ti_3O_{12}/Pt$ bilayer (b) Cross-sectional of the $CoFe_2O_4/Bi_{3.4}La_{0.6}Ti_3O_{12}/Pt$ bilayer (c) $CoFe_2O_4/Bi_{3.4}La_{0.6}Ti_3O_{12}/Pt$ four-layer and (d) $CoFe_2O_4/Bi_{3.4}La_{0.6}Ti_3O_{12}/Pt$ ten-layer structures*

b. Electric Properties

The value of leakage current is usually one of the most critical factors for FeRAMs (ferroelectric random access memories) application of ferroelectric thin films, due to its direct relation to power consumption and function failure of devices. The leakage current was measured by Keithley 6514 electrometer in order to understand the porosity effect of

electroceramics. The capacitor structure (Figure 4.5) were used all measurements were performed at room temperature in the voltage range of 0.2 V to 10 V and delay time of 10s.

Figure 4.4 shows the leakage current density (J) as a function of applied dc electric field on the capacitor structure of $CoFe_2O_4/Bi_{3.4}La_{0.6}Ti_3O_{12}/Pt$ bilayer, four-layer and ten-layer structures. In electroceramics such as $Bi_{4-x}M_xTi_3O_{12}$ (M = La and Sm) [4] leakage current were observed to be controlled by the bulk state, i.e., ohmic behavior in low fields, and in the intermediate field grain boundaries regions may be effective, but in very large fields, space charge limited current (SCLC) and electrode-film interface resistance may dominate [4], [35].

As can be observed in Figure 4.4, the leakage current of $CoFe_2O_4/Bi_{3.4}La_{0.6}Ti_3O_{12}$ /Pt bilayer structure also follows similar behavior. Leakage current is low (below 10^{-6} A) up to applied field 90 kV/cm, and it shows an ohmic response. Under certain intermediate field~ 150 KV/cm, the point of inflexion is observed and current shoots up to 10^{-4} A at higher electric field the power law follows and then the dielectric breakdown occurs, because bilayer film thickness is large (550 nm), space charge limited current (SSLC) is not applicable.

For $CoFe_2O_4/Bi_{3.4}La_{0.6}Ti_3O_{12}/Pt$ four-layer structure leakage current is below 10^{-5} A and shows Ohmic behavior in low field (90 KV/cm. Leakage current can be attributed to defect such as oxygen vacancies interacting strongly with domain boundaries, which should have significant influences on the conduction process.

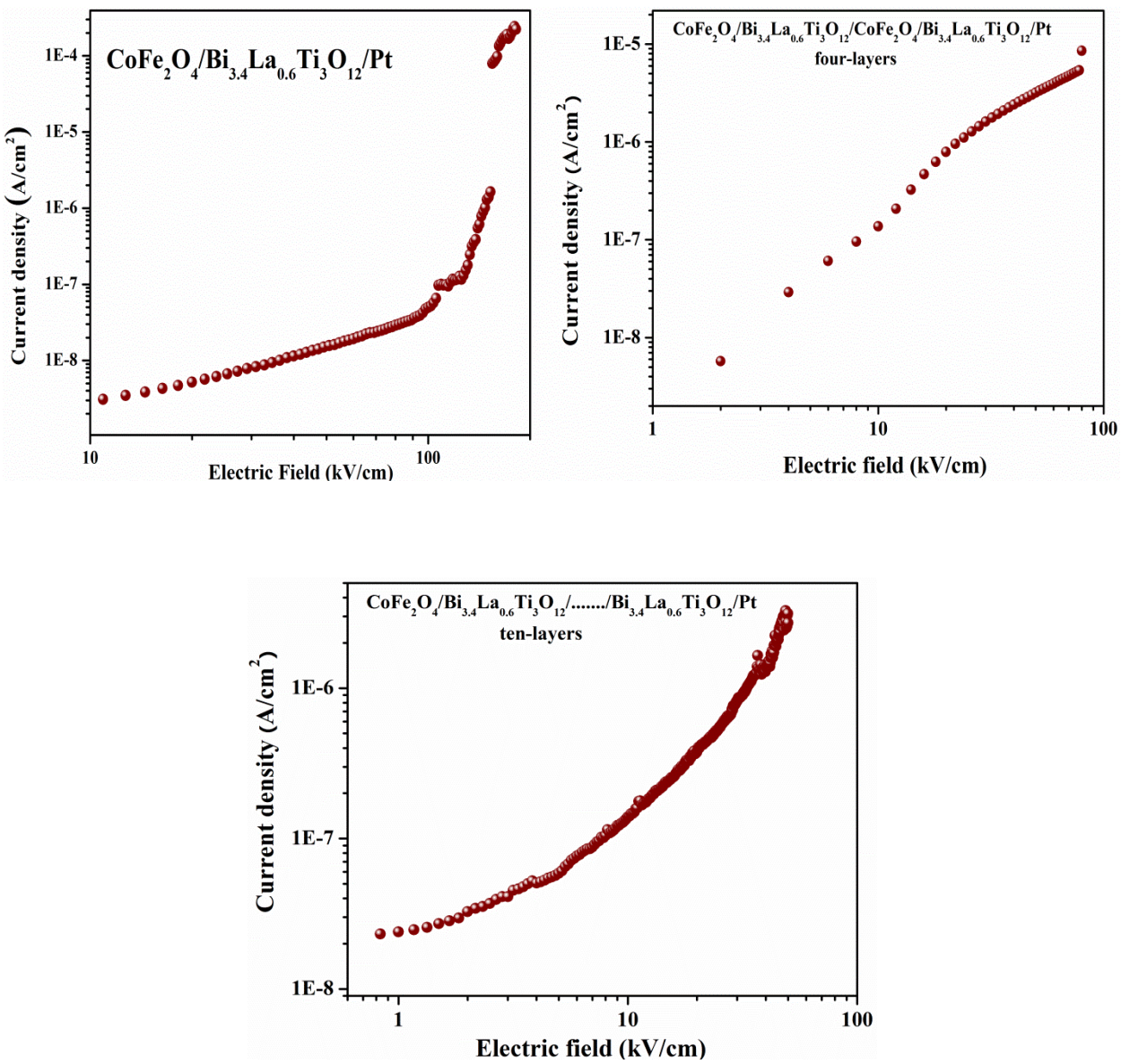

Figure 4. 4 *Leakage current versus electric field of $CoFe_2O_4/Bi_{3.4}La_{0.6}Ti_3O_{12}$ /Pt bilayer, four-layer and ten-layer structure.*

For $CoFe_2O_4/Bi_{3.4}La_{0.6}Ti_3O_{12}$/Pt ten-layer structure leakage current is below 10^{-5} A in low field region (< 90 KV/cm), and it follows Ohmic behavior. Because multilayer thickness is large the inflexion and tunneling phenomena can be ruled out and non-linear Ohmic conduction due to Poole Frankel effect is not valid.

$CoFe_2O_4/Bi_{3.4}La_{0.6}Ti_3O_{12}/Pt$ multilayers were also characterized for dielectric responses. These properties were measured with capacitors fabricated with the ferroelectric materials as a function of applied frequency. Capacitors were fabricated depositing Pt top electrodes, i.e. *Pt-ferroelectric thin film-Pt* structure. The ferroelectric materials are in general characterized by higher dielectric constant approximately (200-10000) and low dielectric loss (Tan δ). Dielectric properties of perovskite structure provide information necessary for the selection of these materials for specific applications and useful in the fabrication new devices.

The electrical capacitor is represented in the Figure 4.5. The Pt top electrode is connected to terminal A, while other electrode is Pt sub layer is connected to the terminal B. Swept harmonic signal of variable frequency is applied and therefore the value of capacitance can be measured.

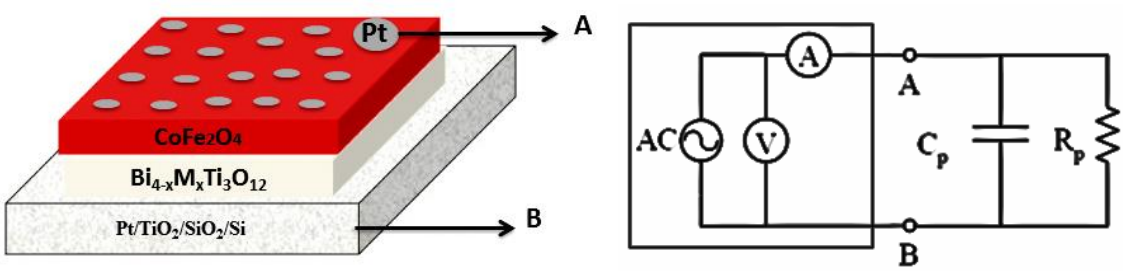

Figure 4. 5 *Vertical schematic of capacitive structure.*

The capacitor has a capacitance C expressed by:

$$C = \frac{\varepsilon_0 \varepsilon A}{d} \qquad \textbf{(13)}$$

Where A is an area of electrode ($3x10^{-4}$ cm^2), ε is dielectric permittivity, d is the thickness of the films, ε_0 is the permittivity of vacuum with value of ($8.8542x10^{-12}$ C^2/Nm^2) and C is capacitance measured. Hence the dielectric permittivity of the material can be extracted from the

direct measurement of the capacitance. From equation (13), the dielectric permittivity can be determined from:

$$\varepsilon = \frac{Cd}{\varepsilon_0 A} \quad \textbf{(14)}$$

Dielectric response and dielectric loss (tan δ) were recorded by impedance analyzer HP 4294a in the range (10^3 - 10^6 Hz) and (-10V to 10V) respectively.

Figure 4.6 shows the dielectric constant and dielectric loss (tan δ) dependent frequency in range of (10^2 Hz – 10^6 Hz) of $CoFe_2O_4/Bi_{3.4}La_{0.6}Ti_3O_{12}/Pt$ bilayer, four-layer and ten-layer structure at room temperature.

In multilayers, the dielectric properties are explained assuming that a heterogeneous structure consisting of grains and grain boundaries exist. Dielectric relaxation is observed, in general. The results indicated that the dielectric constant decrease with the thickness of films.

For $CoFe_2O_4/Bi_{3.4}La_{0.6}Ti_3O_{12}/Pt$ ten-layer structure dielectric constant greater that 1500 at low frequency 10^2 Hz and decreases abruptly to 450 at frequency < 10^4 Hz. The dielectric relaxation occurs at frequencies in the range 10^4 Hz – 10^6 Hz. For $CoFe_2O_4/Bi_{3.4}La_{0.6}Ti_3O_{12}/Pt$ four-layer structure shows dielectric constant loss than 850 at low frequency 10^2 Hz and dielectric relaxation complete occurs to high frequency 10^6 Hz. For $CoFe_2O_4/Bi_{3.4}La_{0.6}Ti_3O_{12}/Pt$ bilayer structure the dielectric relaxation occurs in frequency range 10^2 Hz – 10^4 Hz and monotonically with increased frequency, exhibiting a typical characteristic of space charge relaxation [66].

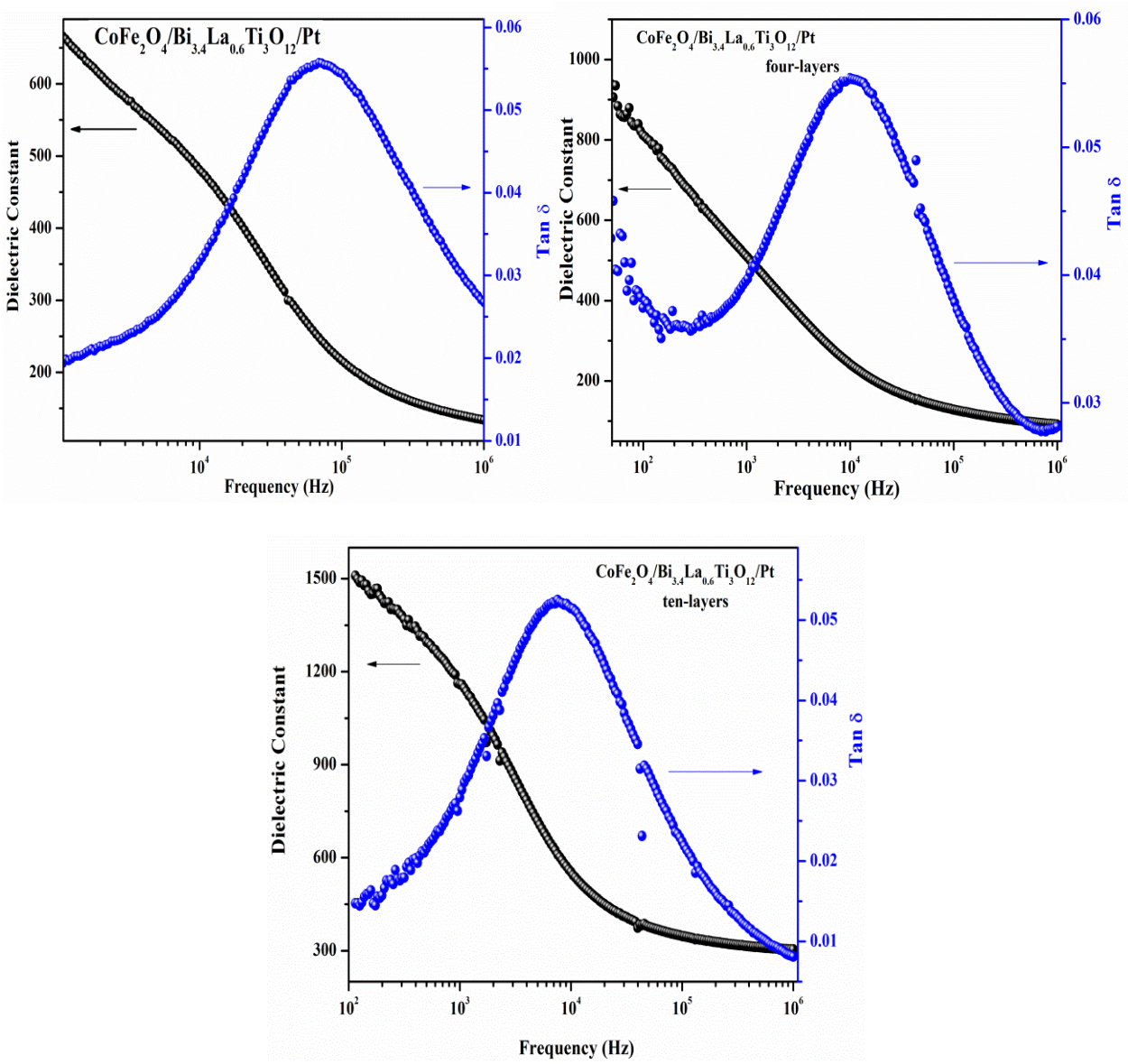

Figure 4. 6 *Dielectric constants vs. frequency response of $CoFe_2O_4/Bi_{3.4}La_{0.6}Ti_3O_{12}/Pt$ bilayer, four-layer and ten-layer structure.*

In these cases of multilayers structure the existence of a large number of interface dipoles and presence of different grain in the boundary can give rise to different relaxation processes. Dielectric loss (tan δ) versus frequency is shows in figure 4.6 for all samples. For $CoFe_2O_4/Bi_{3.4}La_{0.6}Ti_3O_{12}/Pt$ bilayer, four-layer and ten-layer structures the dielectric loss follows similar behavior. Increased in frequency range (10^2 Hz - >10^4 Hz) then maximizes frequency in

range <10^4 Hz to 10^5 Hz and minimizes to less than 3% at 10^6 Hz for all structure. We can observe that in ten-layer structure, the dielectric loss is below 1% in comparison to the loss in bilayer and four-layer structures. This anomaly is attributed due to the polycrystalline nature of multilayer structures and may be explained theoretically by consideration of the Maxwell-Wagner two-layer model [66].

The ferroelectric characterization of the multilayers materials was carried out by measuring of the polarization as a function of the applied electric field. The ferroelectric response was tested using RT 6514 HVS tester. The top platinum (Pt) electrodes, of diameter ($3x10^{-4}$ cm^2) were deposited by dc sputtering using mechanical mask for the measurements of ferroelectric response. All samples were applied a frequency range from 100 Hz to 1 KHz and a voltage 10V. Figure 4.7 shows the polarization-electric field (P-E) hysteresis loops of pure $Bi_{3.4}La_{0.6}Ti_3O_{12}$ (BLT) film, $CoFe_2O_4/Bi_{3.4}La_{0.6}Ti_3O_{12}$ bilayer, four-layer and ten-layer structures. As shown in Table 2. The thickness of $Bi_{3.4}La_{0.6}Ti_3O_{12}$ is ~ 250 nm (measured by profilometer). Hysteresis loops for $CoFe_2O_4/Bi_{3.4}La_{0.6}Ti_3O_{12}$ bilayer, four-layer and ten-layer structures show well-saturated ferroelectric response with remnant polarization shows in Table 2. Large value of ferroelectric remnant polarization and saturation polarization in $CoFe_2O_4/Bi_{3.4}La_{0.6}Ti_3O_{12}$ bilayer suggests preferred orientation in the c-axis like the $Bi_4Ti_3O_{12}$ phase.

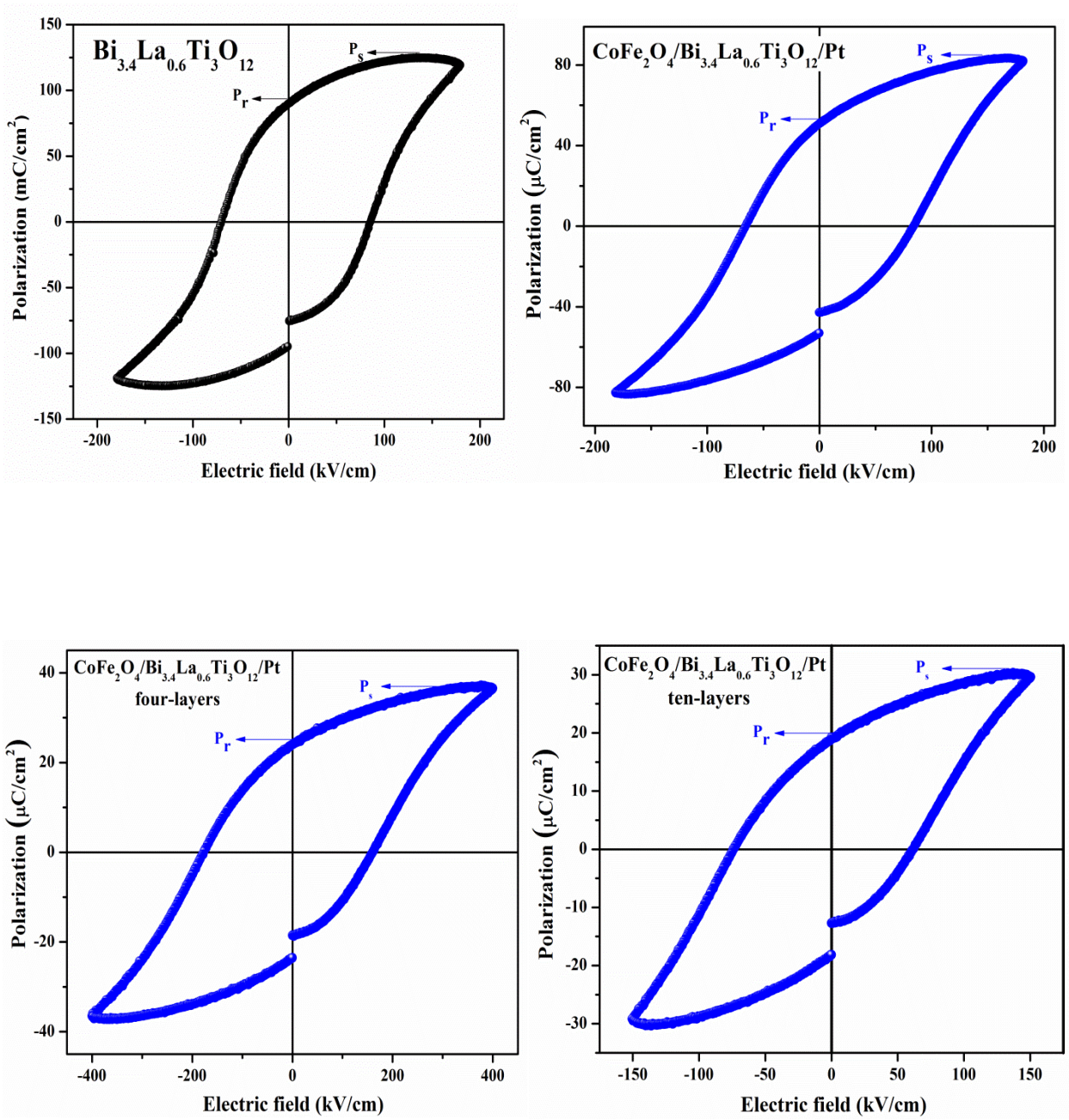

Figure 4. 7 *Ferroelectric hysteresis loop of pure $Bi_{3.4}La_{0.6}Ti_3O_{12}$/Pt film and $CoFe_2O_4/Bi_{3.4}La_{0.6}Ti_3O_{12}$/Pt bilayer, four-layer and ten-layer structures*

For $CoFe_2O_4/Bi_{3.4}La_{0.6}Ti_3O_{12}$/Pt four-layer and ten-layer structure hysteresis loops shows spontaneous polarization values are lower as compared to $Bi_{3.4}La_{0.6}Ti_3O_{12}$ and bilayer structure,

(see Table 2). This is due to the presence the intermediate $CoFe_2O_4$ dielectric layers along with the ferroelectric $Bi_{3.4}La_{0.6}Ti_3O_{12}$ layer. It is observed that higher amount of layers degrades the electrical polarization due to the presence of non-ferroelectric $CoFe_2O_4$ region.

Table 2 *Values of remnant polarization and saturation polarization of pure films and multilayers structures*

Thin film	Remnant polarization P_r (μC/cm^2)	Saturation polarization P_s (μC/cm^2)
$Bi_{3.4}La_{0.6}Ti_3O_{12}$	93	128
$CoFe_2O_4/Bi_{3.4}La_{0.6}Ti_3O_{12}$ bilayer	53	85
$CoFe_2O_4/Bi_{3.4}La_{0.6}Ti_3O_{12}$ four-layer	26	39
$CoFe_2O_4/Bi_{3.4}La_{0.6}Ti_3O_{12}$ ten-layer	20	32

However, to confirm and understanding these results we deposited four-layer films on Pt with different thicknesses of $Bi_{3.4}La_{0.6}Ti_3O_{12}$ and $CoFe_2O_4$ where $Bi_{3.4}La_{0.6}Ti_3O_{12}$ layer was first deposited on Pt substrate, as shown in Figure 4.8. Multilayer films were prepared under same conditions that all films above and characterized by ferroelectric hysteresis loops at room temperature. Figure 4.9 shows comparison hysteresis loops of $CoFe_2O_4/Bi_{3.4}La_{0.6}Ti_3O_{12}$/Pt four-layers where $Bi_{3.4}La_{0.6}Ti_3O_{12}$ thick layers and $CoFe_2O_4$ thin layers.

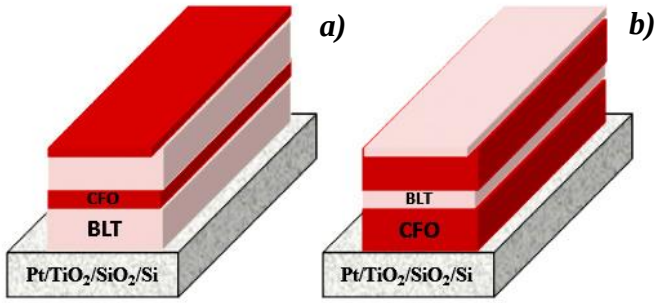

Figure 4. 8 *Multilayer structures of $CoFe_2O_4/Bi_{3.4}La_{0.6}Ti_3O_{12}/Pt$ four-layer with (a) $Bi_{3.4}La_{0.6}Ti_3O_{12}$ layers thicker and (b) $CoFe_2O_4$ layers thicker*

As shown in figure 4.9 (a), the value larger remnant polarization P_r= 30 μC/cm^2 corresponds at multilayer structure containing $Bi_{3.4}La_{0.6}Ti_3O_{12}$ layers thicker.

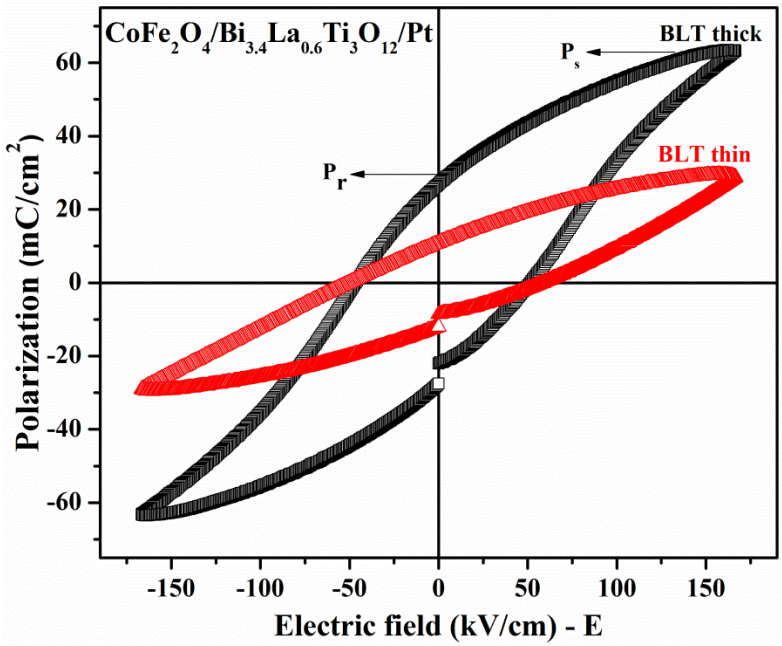

Figure 4. 9 *Comparison ferroelectric hysteresis loops of $CoFe_2O_4/Bi_{3.4}La_{0.6}Ti_3O_{12}/Pt$ four-layer of $Bi_{3.4}La_{0.6}Ti_3O_{12}$ layers thicker and $CoFe_2O_4$ layers thicker.*

Figure 4.9 directly indicates that larger is the thickness of $Bi_{3.4}La_{0.6}Ti_3O_{12}$ in comparison to $CoFe_2O_4$ large ferroelectric response. This is attributed behavior of a composite.

On the other hand the small gap in end of the hysteresis loops can be attributed to the adhesion problem of top Pt contact electrodes and some pores present in the surface of film, a possible solution to these problems would be the post annealing of the electrodes, before measurement and increased time of drying.

c. Magnetic Properties

Figure 4.10 shows the comparison of typical magnetic hysteresis loop (M-H) for pure $CoFe_2O_4$/Pt film (a) and of $CoFe_2O_4/Bi_{3.4}La_{0.6}Ti_3O_{12}$/Pt (b) bilayer structure, measured by Vibrating Sample Magnetometer (VSM) at room temperature with magnetic fields up to 16 kG applied parallel to the sample plane.

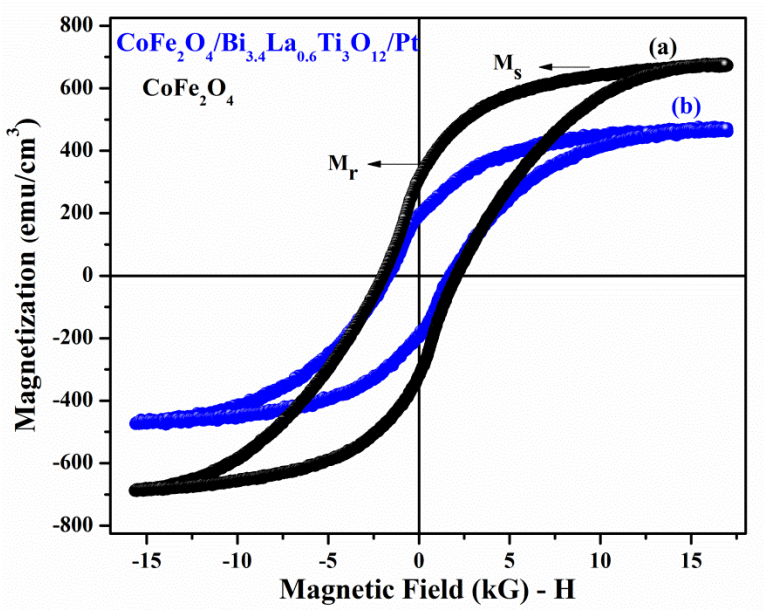

Figure 4. 10 *M-H loops the comparison of (a) pure $CoFe_2O_4$/Pt film and (b) $CoFe_2O_4/Bi_{3.4}La_{0.6}Ti_3O_{12}$/Pt bilayer structure.*

The pure $CoFe_2O_4$ films exhibited a predominant ferrimagnetic behavior with large value in magnetic saturation (> 600 emu/cm^3). Bilayer structure exhibited ferrimagnetic behavior well saturated magnetization; values are shown in Table 3, i.e. composite bilayer is ferrimagnetic.

These results evidence formation the $CoFe_2O_4$ spinel structure in bilayer structure. Figure 1.11 shows for comparison, $CoFe_2O_4/Bi_{3.4}La_{0.6}Ti_3O_{12}/Pt$ four-layer and ten-layer structures the ferromagnetic hysteresis shows low remnant magnetization in comparison with bilayer structure, see value in table 3. The coercivity and saturation magnetization values decreases with amount $CoFe_2O_4$ layers in multilayer, however the formation of $CoFe_2O_4$ spinel structure revealed for x-ray measurement is confirm in hysteresis loops well-definition and perfectly saturated. The different value of the magnetic saturation between multilayer are be associated at interaction between different layers involved.

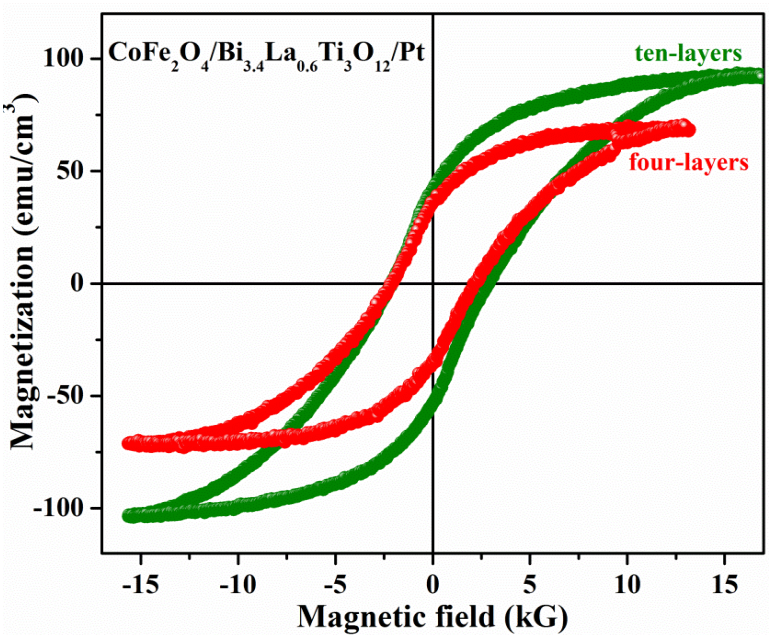

Figure 4. 11 *M-H loops the comparison of $CoFe_2O_4/Bi_{3.4}La_{0.6}Ti_3O_{12}/Pt$ four-layer and ten-layer structures.*

Table 3 *Values of remnant, saturation magnetization and coercive field of pure $CoFe_2O_4$, bilayers, four and ten-layer structure.*

Thin film	Magnetization M_r (emu/cm^3)	Magnetic Saturation M_s (emu/cm^3)	Coercive Field H_c (kG)
$CoFe_2O_4$/Pt	328	688	2.1
$CoFe_2O_4/Bi_{3.4}La_{0.6}Ti_3O_{12}$ bilayer	206	480	1.8
$CoFe_2O_4/Bi_{3.4}La_{0.6}Ti_3O_{12}$ four-layer	40	72	
$CoFe_2O_4/Bi_{3.4}La_{0.6}Ti_3O_{12}$ ten-layer	47	96	

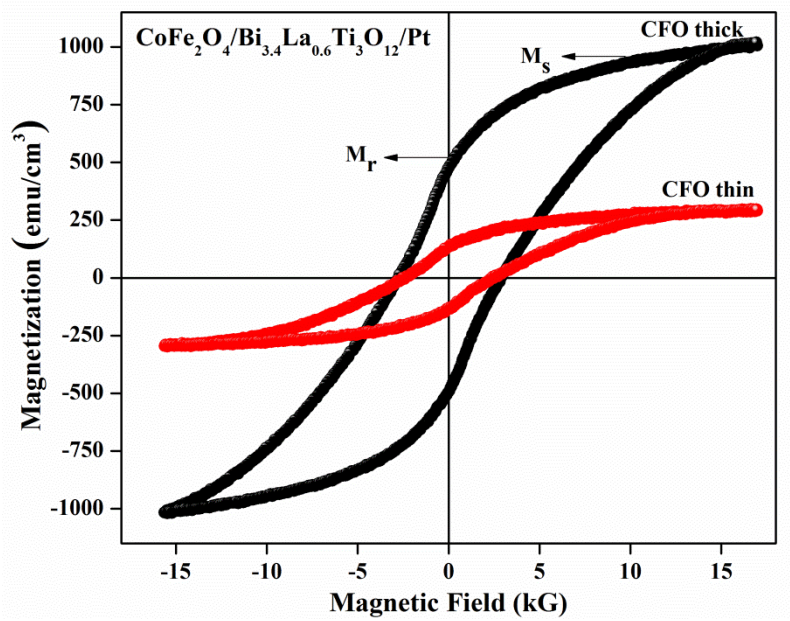

Figure 4. 12 *M-H loops the comparison of $CoFe_2O_4/Bi_{3.4}La_{0.6}Ti_3O_{12}$/Pt four-layer of $Bi_{3.4}La_{0.6}Ti_3O_{12}$ layers thicker and $CoFe_2O_4$ layers thicker.*

Comparison of ferromagnetic response of four-layer with $CoFe_2O_4$ (thicker) and $Bi_{3.4}La_{0.6}Ti_3O_{12}$ (thicker) and vice versa is shown in Figure 4.12. One can observe high saturation

magnetization when $CoFe_2O_4$ layers are thicker in multilayer structure. This is again the behavior of composite. Thus, all multilayers are composite whose properties can be tuned.

Concluding Remarks

X-ray results in pure film suggested the partial substitution of lanthanum La^{3+} on Bi^{3+} ion in $Bi_{3.4}La_{0.6}Ti_3O_{12}$ and the formation $CoFe_2O_4$ spinel structure. With carefully controlled stoichiometry of the spin coated films, x-ray revealed the formation of composite-like structure in multilayer. Peaks present in multilayer corresponds at perovskite and spinel phase. SEM revealed that films are polycrystalline does show neither cracks nor vacancies.

Electrical properties of multilayer structure are shows in ferroelectric hysteresis loops, dielectric constant and leakage current. The leakage current is low below 10^{-5} A for most samples and shows Ohmic behavior occurs at low fields. The dielectric response shows dielectric relaxation, which indicates change in crystal structure in composite. Dielectric loss, tan (δ), is small around 1-3% at 10^{-6} Hz for all samples. Relaxation is attributed to different resistivity and permittivity of the layers involved. It will need more studies confirm.

Co-existence of ferromagnetic and ferroelectric coupling order parameters in the same multilayer structures was demonstrated for the system $CoFe_2O_4/Bi_{3.4}La_{0.6}Ti_3O_{12}$ with large spontaneous polarization and magnetization values. Such composite layers can used a bi-functional memory, and need to be investigated further in device structures.

4.2 $CoFe_2O_4/Bi_{3.4}Sm_{0.6}Ti_3O_{12}$/Pt multilayer structure

To reinforce the concept of composites, we also investigated bilayers and four-layer structure of $CoFe_2O_4/Bi_{3.4}Sm_{0.6}Ti_3O_{12}$/Pt were deposited on Pt substrate under same conditions that all films above. We report here the structural, dielectric responses, and the co-existence of well saturated ferroelectric and ferromagnetic responses of multilayer films a room temperature.

a. Structural Properties

$CoFe_2O_4/Bi_{3.1}Sm_{0.9}Ti_3O_{12}$/Pt was characterized by x-ray diffraction showing polycrystalline growth as observed in Figure 4.13. For comparison, the x-ray diffraction patterns of $CoFe_2O_4$/Pt and $Bi_{3.4}Sm_{0.6}Ti_3O_{12}$/Pt is included with $CoFe_2O_4/Bi_{3.4}Sm_{0.6}Ti_3O_{12}$/Pt bilayer structure and $CoFe_2O_4/Bi_{3.4}Sm_{0.6}Ti_3O_{12}$/Pt four-layer. The average thicknesses of the films were 340 nm for the bilayer, 500 nm for four-layer and 670 nm for ten-layer structures.

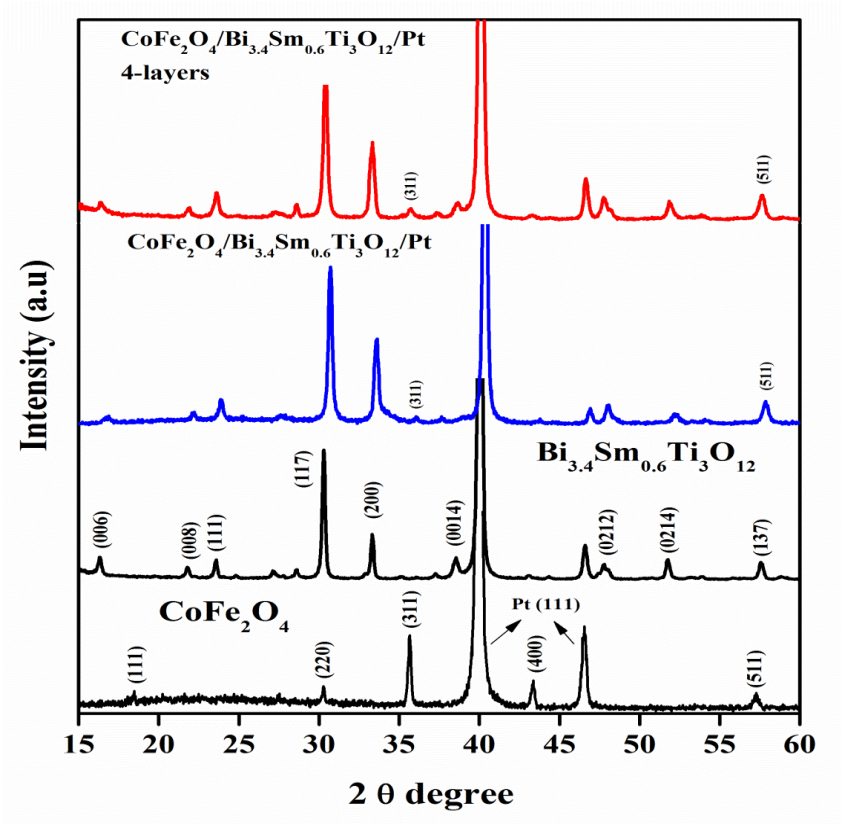

Figure 4. 13 *X-ray diffraction patterns of $CoFe_2O_4$, $Bi_{3.4}Sm_{0.6}Ti_3O_{12}$ films, $CoFe_2O_4$/ $Bi_{3.4}Sm_{0.6}Ti_3O_{12}$ bilayer structure and $CoFe_2O_4$/ $Bi_{3.4}Sm_{0.6}Ti_3O_{12}$ four-layer structure*

X-ray indicates that the Sm^{3+} ion partially replaces the Bi^{3+} ion in $Bi_4Ti_3O_{12}$ perovskite structure. The predominant x-ray diffraction peaks (117) and (200) of $Bi_{3.4}Sm_{0.6}Ti_3O_{12}$ and (311) and (511) peaks of $CoFe_2O_4$ co-exist in the bilayer and four-layer structures. X-ray diffraction of the bilayer and four-layer system revealed the composite-like structure.

Figure 4.14 shows the scanning electron microscopy (SEM) for $CoFe_2O_4$/$Bi_{3.4}Sm_{0.6}Ti_3O_{12}$/Pt bilayer and four-layer structures. Images shows polycrystalline films with grain size uniform and the surfaces morphology did not present cracks or defects indicating the deposition of homogeneous films.

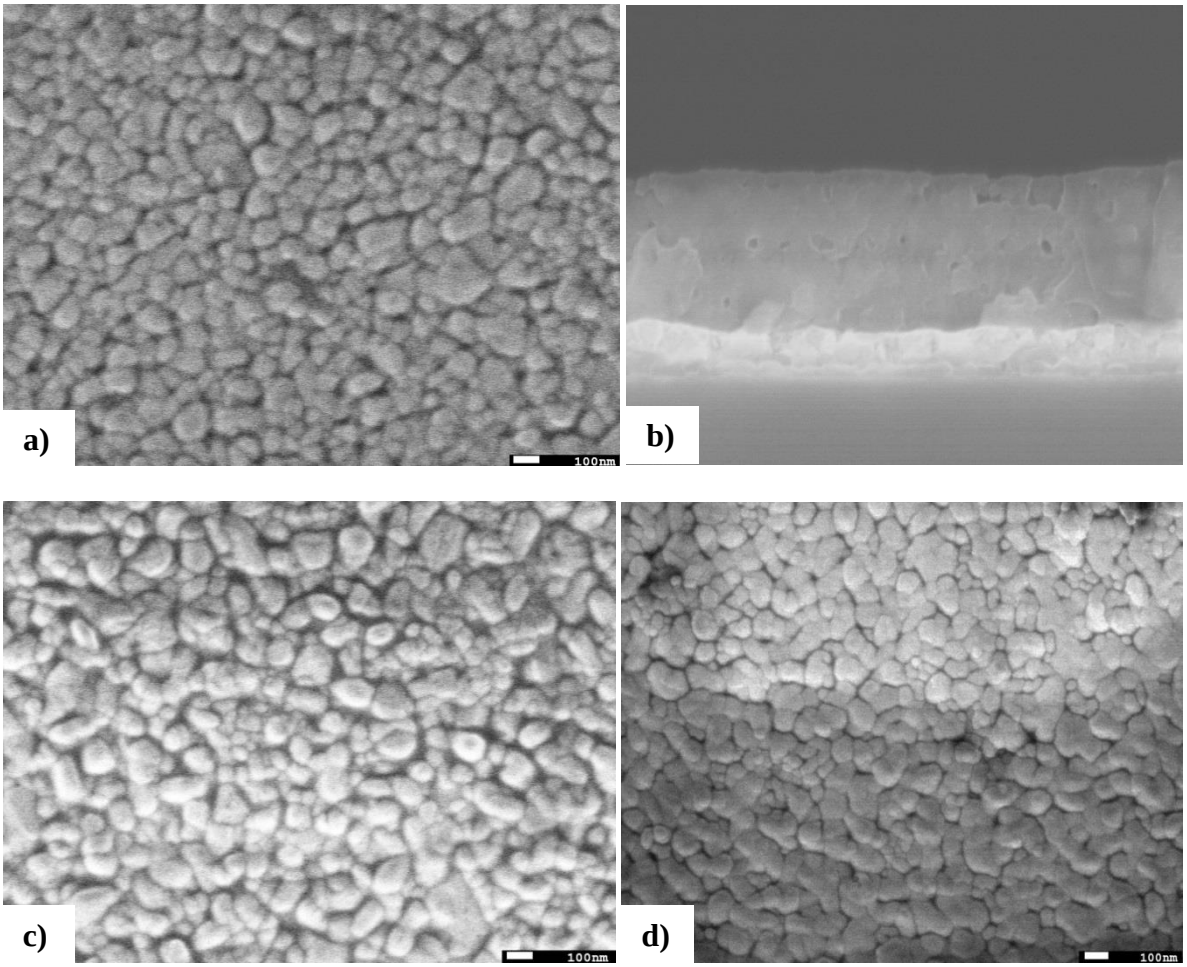

Figure 4. 14 *SEM micrograph showing surfaces morphology of (a) $CoFe_2O_4/Bi_{3.4}Sm_{0.6}Ti_3O_{12}/Pt$ bilayer, (b) Cross-sectional of the bilayer structure (c) $CoFe_2O_4/Bi_{3.4}Sm_{0.6}Ti_3O_{12}/Pt$ four-layer structures and (d) $CoFe_2O_4/Bi_{3.4}Sm_{0.6}Ti_3O_{12}/Pt$ ten-layer structures*

b. Electric Properties

Figure 4.15 shows the frequency dependencies of the dielectric constant and loss tangent (Tan δ) in the frequency range of 10^2 Hz - 10^6 Hz of $CoFe_2O_4/Bi_{3.4}Sm_{0.6}Ti_3O_{12}$. For ten-layer structure dielectric constant is higher (1400) at low frequency 10^2 Hz and at frequency range $>10^2$ Hz to 10^5 Hz decreases abruptly shows a dielectric relaxation.

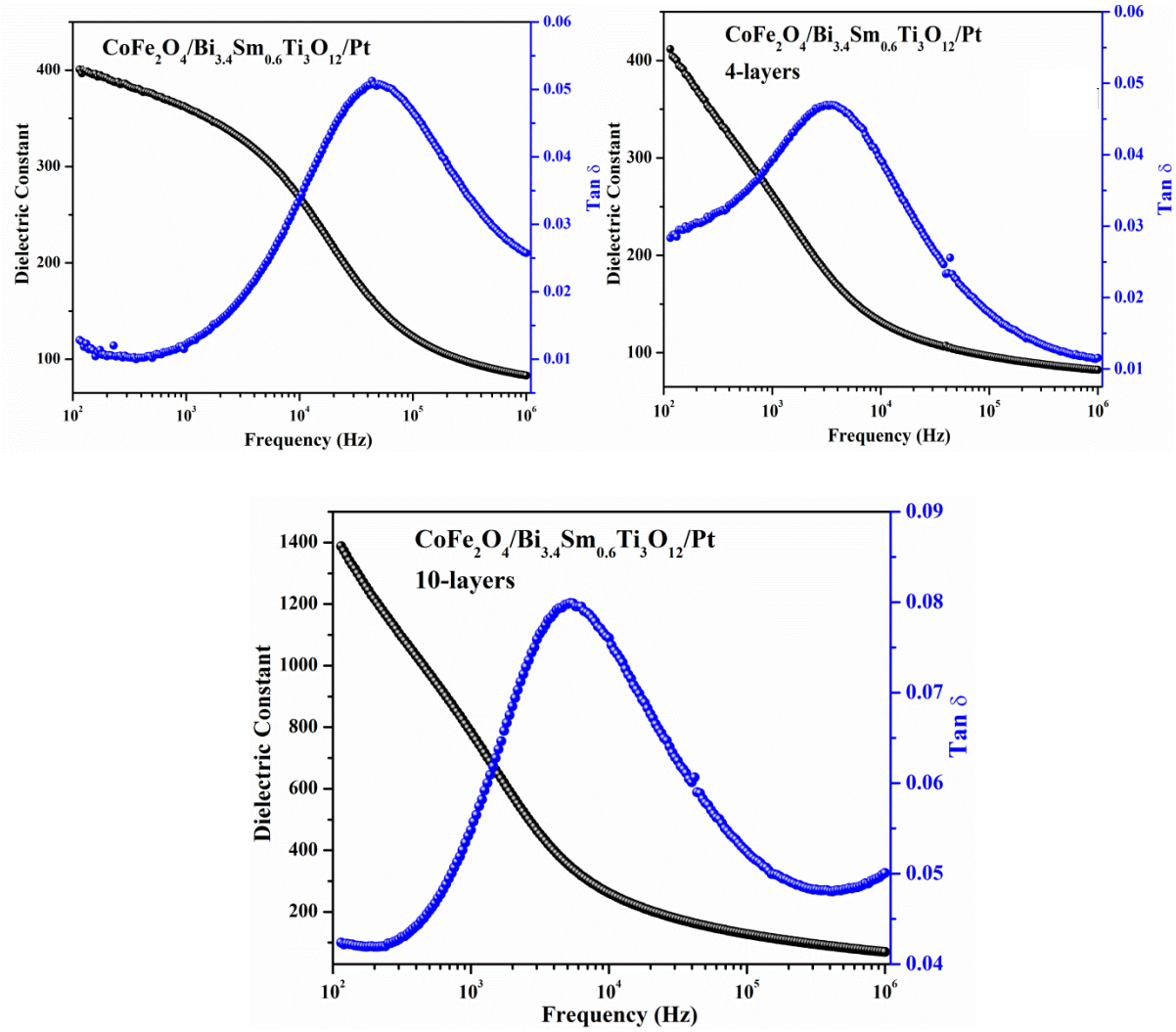

Figure 4. 15 *Dielectric constant versus frequency of $CoFe_2O_4/Bi_{3.4}Sm_{0.6}Ti_3O_{12}/Pt$ bilayer and four-layer structures.*

For for-layer structure dielectric constant decreases from 400 to 80 in frequency range (10^2 Hz - 10^6 Hz) exhibiting a typical characteristic of space charge relaxation. A similar behavior shown bilayer structure these results could attributed at thickness of films. On the other hand dielectric loss (tan δ) is less than 3% for all samples. For ten-layer dielectric loss maximize

in 10^4 Hz and frequency (< 10^4 Hz) shows dielectric loss relaxation around 2%. For four-layer structure dielectric loss maximized between frequency 10^3 – 10^4 Hz and next decrease showing dielectric loss relaxation to 1%. The maximized value of dielectric loss for bilayer structure occurs at 10^5 Hz. These results suggest that amount of layers involved increases dielectric loss a definite frequency range. Measurements for $CoFe_2O_4/Bi_{3.4}Sm_{0.6}Ti_3O_{12}$ system are consistent with those previously obtained in system $Bi_{3.4}La_{0.6}Ti_3O_{12}$ system.

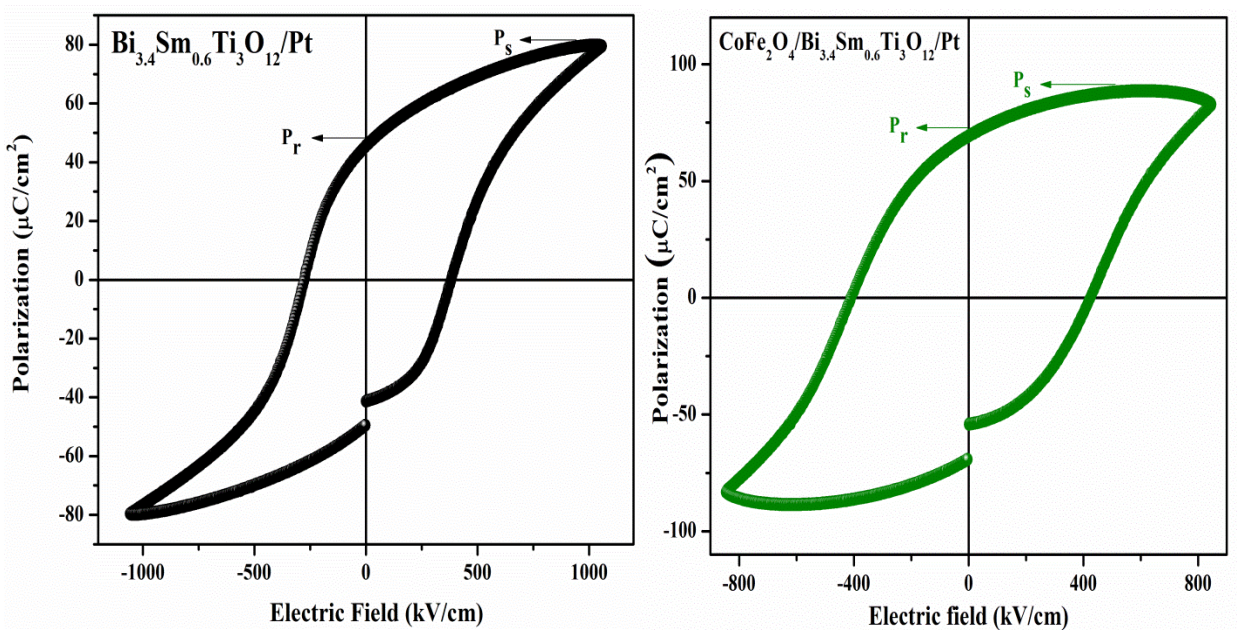

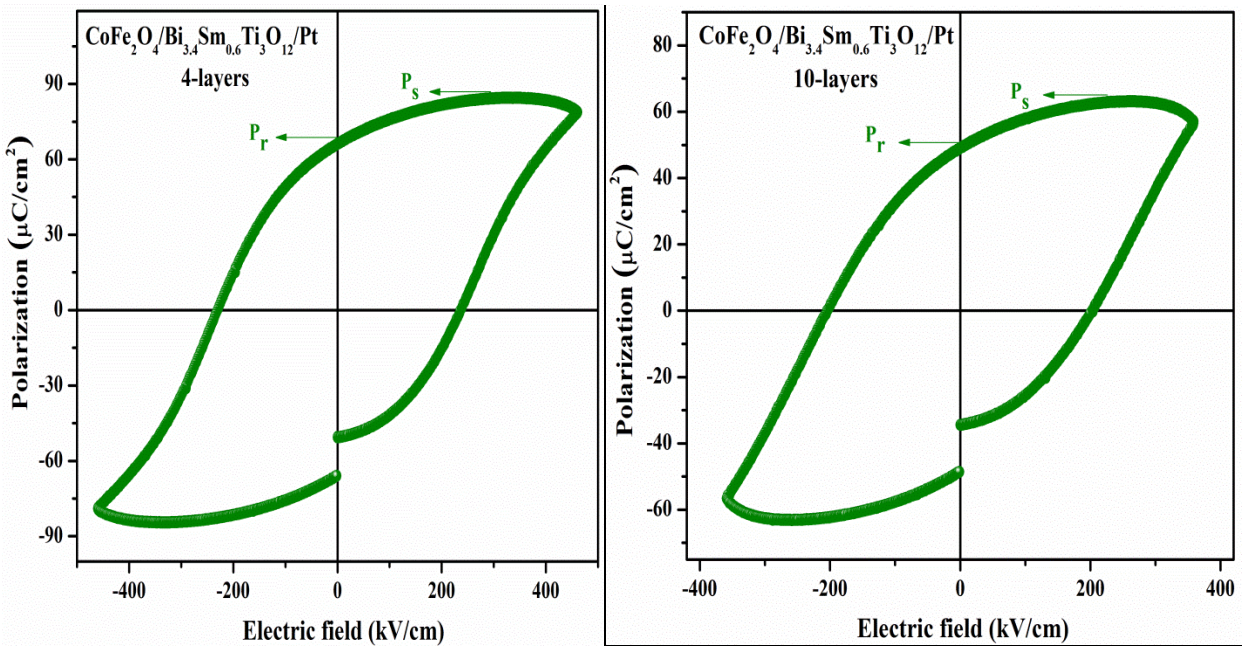

Figure 4. 16 *Ferroelectric hysteresis loop of pure $Bi_{3.4}Sm_{0.6}Ti_3O_{12}$/Pt film and $CoFe_2O_4/Bi_{3.4}Sm_{0.6}Ti_3O_{12}$/Pt bilayer, four-layer and ten-layer structures*

Figure 4.16 shows the polarization-electric field (P-E) hysteresis loops of pure $Bi_{3.4}Sm_{0.6}Ti_3O_{12}$ structure and $CoFe_2O_4/Bi_{3.4}Sm_{0.6}Ti_3O_{12}$ bilayer, four-layer and ten-layer structures. The measurement was obtained with applied voltage 30 V for all samples. Pure $Bi_{3.4}Sm_{0.6}Ti_3O_{12}$ shows formation of perovskite structure with large remnant and saturated polarization are shows in Table 4. As evidence for obtained results remnant polarization values decreases with increasing amount layers deposited. This result was consistent with those previously obtained in system $CoFe_2O_4/Bi_{3.4}La_{0.6}Ti_3O_{12}$/Pt. The hysteresis loops for bilayer and four-layer shows great spontaneous polarization and noble saturation, however hysteresis loops for ten-layer structure evidence a decline in saturated polarization and the measured of the polarization are inflated due to the leakage current this can be attributed a porous surface.

Table 4 *Values of remnant polarization and saturation polarization of pure, bilayer, four-layer and ten-layer structures.*

Film	**Remnant Polarization P_r (μC/cm^2)**	**Saturation Polarization P_s (μC/cm^2)**
$Bi_{3.4}Sm_{0.6}Ti_3O_{12}$	49	82
$CoFe_2O_4/Bi_{3.4}Sm_{0.6}Ti_3O_{12}$ bilayer	71	91
$CoFe_2O_4/Bi_{3.4}Sm_{0.6}Ti_3O_{12}$ four-layer	68	87
$CoFe_2O_4/Bi_{3.4}Sm_{0.6}Ti_3O_{12}$ ten-layer	51	~65

c. Magnetic Properties

Figure 4.17 shows the hysteresis loop of $CoFe_2O_4/Bi_{3.4}Sm_{0.6}Ti_3O_{12}$ bilayer, four-layer and ten-layer structures. All films evidenced ferrimagnetic behavior with hysteresis curves well-formed. Corresponding saturated magnetization and remnant magnetization values are shown in Table 5.

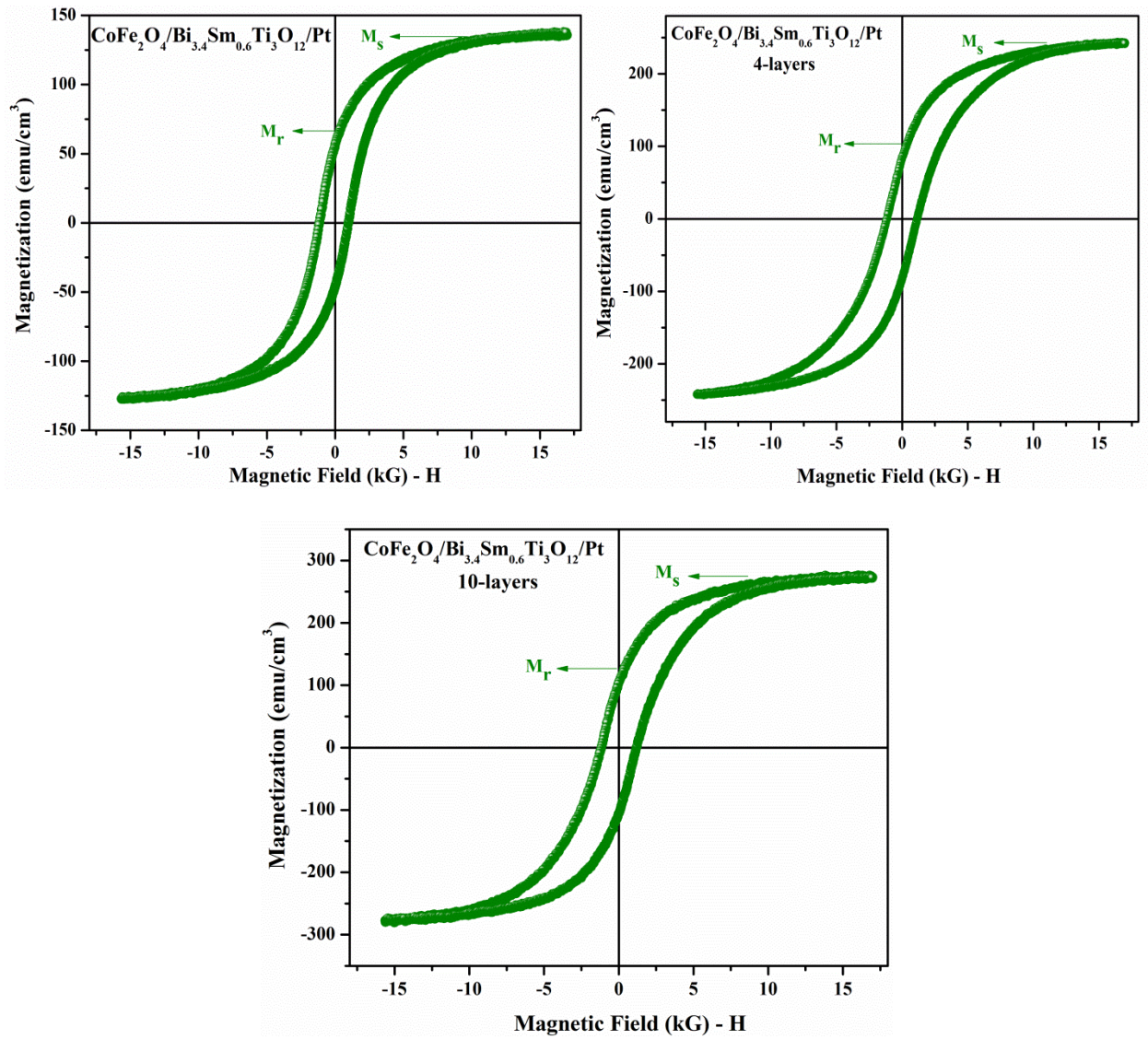

Figure 4. 17 *Ferromagnetic hysteresis loops of $CoFe_2O_4/Bi_{3.4}Sm_{0.6}Ti_3O_{12}$ bilayer, four-layer and ten-layer structures.*

For comparison in values of table 1 the $CoFe_2O_4/Bi_{3.4}Sm_{0.6}Ti_3O_{12}/Pt$ system, presents lower ferromagnetic memory in comparison with $CoFe_2O_4/Bi_{3.4}La_{0.6}Ti_3O_{12}/Pt$ structures. Higher values of remnant magnetization are shown in four-layer film, so that the amount of $CoFe_2O_4$ layers deposited contributes to increasing ferrimagnetic properties in the films.

Table 5 *Values of remnant magnetization and saturated magnetization of bilayers, four-layer and ten-layer structures*

Films	Remnant Magnetization M_r (emu/cm^3)	Saturated Magnetization M_s (emu/cm^3)
$CoFe_2O_4/Bi_{3.4}Sm_{0.6}Ti_3O_{12}$ bilayer	69	141
$CoFe_2O_4/Bi_{3.1}Sm_{0.9}Ti_3O_{12}$ four-layer	103	250
$CoFe_2O_4/Bi_{3.4}Sm_{0.6}Ti_3O_{12}$ ten-layer	121	280

Concluding Remarks

X-ray revealed the formation of composite-like structure in multilayer. SEM revealed that films are polycrystalline. The dielectric response decreases at high frequency. Dielectric loss, tan (δ), is less than 5% all samples. These results suggest that amount of layers involved increases dielectric loss a definite frequency range. Co-existence of ferromagnetic and ferroelectric coupling order parameters in the same multilayer structures was demonstrated for the system $CoFe_2O_4/Bi_{3.4}Sm_{0.6}Ti_3O_{12}$ with large spontaneous polarization and magnetization values. Measurements for $CoFe_2O_4/Bi_{3.4}Sm_{0.6}Ti_3O_{12}$ system are consistent with those previously obtained in system $Bi_{3.4}La_{0.6}Ti_3O_{12}$ system.

V. GENERAL CONCLUSIONS

In this work we have been successfully synthesize of chemical solution route and deposited two type of multilayers $CoFe_2O_4/Bi_{3.4}M_{0.6}Ti_3O_{12}/Pt$ (M= La, Sm) deposited on Pt substrates by spin coating. The existence of a composite-like structure at room temperature is confirmed by x-ray diffraction, Ferroelectric hysteresis loop, Ferromagnetic hysteresis loops, dielectric response and leakage current. Were studied showing ferroelectric and ferromagnetic properties. These materials are potential candidate for FeRAMs (ferroelectric random access memories), MRAMs (magnetic random access memories), non-linear magneto-optical devices, surface acoustic wave devices, tunable capacitors, and sensing applications. SEM morphology shows surface homogeneous without cracks.

Excellent ferroelectric and ferromagnetic properties are obtained in $CoFe_2O_4/Bi_{3.4}M_{0.6}Ti_3O_{12}/Pt$ multilayer films. It showed large values of spontaneous polarization (P_r > 20 μC/cm^2) and remnant magnetization (M_r > 39 emu/cm^3) is observed at room temperature. Leakage current is low and shows ohmic behavior in low fields. Dielectric responses decrease with frequency and the electroceramic materials typical behavior. Co-existence of ferromagnetic and ferroelectric coupling order parameters in the same multilayer structure is attributed to the stress and dielectric relaxation in horizontally aligned structure. For the case multilayer films of Sm-substituted in $Bi_{3.4}M_{0.6}Ti_3O_{12}$ hysteresis loops present large spontaneous polarization (P_r > 40 μC/cm^2) and remnant magnetization (M_r > 70 emu/cm^3).

Although the exact origin of co-existence of ferroelectric and ferromagnetic responses is unclear, stress in multilayers and dielectric relaxation could contribute to ferroelectric and ferromagnetic.

VI. FUTURE PROSPECTIVES

We have demonstrated the ferroelectric and ferromagnetic coupling in bilayers films and multilayers at room temperature. Thus, these materials are potentially candidate for FeRAMs (ferroelectric random access memories). Substrate-film interface effect, grain boundaries in multilayer structures and its effect on multiferroic properties need to be studied further.

The following future work is required:

- ✓ To optimize the film thickness and its effect on ferroelectric and ferromagnetic coupling parameters.
- ✓ Study of relaxation by changing different contact sizes
- ✓ Fabricate the FeRAM structure with suitable interfacial layer.

REFERENCES

[1] L. W. Martin, Y.-H. Chu, and R. Ramesh, “Advances in the growth and characterization of magnetic, ferroelectric, and multiferroic oxide thin films,” *Mater. Sci. Eng. R Reports*, vol. 68, no. 4–6, pp. 89–133, May 2010.

[2] “B. Auriv-illius, Mixed bismuth oxides with layer lattices: II. Structure of Bi4Ti3O12,” *Ark. Kemi*, vol. 1, no. 463, 1949.

[3] T. Kojima, T. Sakai, T. Watanabe, H. Funakubo, K. Saito, and M. Osada, “Large remanent polarization of (Bi,Nd)[sub 4]Ti[sub 3]O[sub 12] epitaxial thin films grown by metalorganic chemical vapor deposition,” *Appl. Phys. Lett.*, vol. 80, no. 15, p. 2746, Apr. 2002.

[4] M. S. Tomar, R. E. Melgarejo, and S. P. Singh, “Leakage current and ferroelectric memory in Nd and Sm substituted Bi4Ti3O12 films,” *Microelectronics J.*, vol. 36, no. 3–6, pp. 574–577, Mar. 2005.

[5] D. Barrionuevo, S. P. Singh, and M. S. Tomar, “Multiferroic Properties of Bi 4−x Nd x Ti 3 O 12 /CoFe 2 O 4 Composite Films,” *Integr. Ferroelectr.*, vol. 124, no. 1, pp. 48–52, Jan. 2011.

[6] M. T. C. Ming-Wen Chu, Marcel Ganne and and L. Brohan, “X-ray photoelectron spectroscopy and high resolution electron microscopy studies of Aurivillius compounds: Bi4ÀxLax Ti3O12 „xÄ0, 0.5, 0.75, 1.0, 1.5, and 2.0….” .

[7] and T. V. R. Ramesh, K. Luther, B. Wilkens, D. L. Hart, E. Wang, J. M. Tarascon, A. Inam, X. D. Wu, “Epitaxial growth of ferroelectric bismuth titanate thin films by pulsed laser deposition,” *Appl. Phys. Lett.*, vol. 57, no. 15, pp. 1505–1508, 1990.

[8] B. Yang, Z. Li, Y. Gao, Y. Lin, and C.-W. Nan, “Multiferroic properties of Bi3.15Nd0.85Ti3O12–CoFe2O4 bilayer films derived by a sol–gel processing,” Elsevier B.V., 2011.

[9] H. M. Rosenberg, *The Solid State*, Third edit. Oxford: Oxford University Press, 1988, p. 315.

[10] R. Rose, L. Shepard, and J. Wulff, *The Structure and Properties of Materials*, Third edit. JOHN WILEY & SONS, INC, 1967, p. 263.

[11] K. Uchino, “Ferroelectric Devices,” *Univ. Park. Pennsylvania*, 2005.

[12] M. E. Lines and A. M. Glass, “Applications of Ferroelectric and Related Materials,” *Oxford Univ. Press. Oxford*, 2004.

[13] Y. H. Hou, Y. J. Zhao, Z. W. Liu, H. Y. Yu, X. C. Zhong, W. Q. Qiu, D. C. Zeng, and L. S. Wen, "Structural, electronic and magnetic properties of partially inverse spinel CoFe 2 O 4 : a first-principles study," *J. Phys. D. Appl. Phys.*, vol. 43, no. 44, p. 445003, Nov. 2010.

[14] R. J. Hill, J. R. Craig, and G. V Gibbs, "No Title," *Phys. Chem. Miner.*, vol. 4, p. 317, 1979.

[15] V. A. M. Brabers, "Handbook of Magnetic Materials," *Elsevier Sci.*, vol. 8, 1997.

[16] E. Paul P, "Foundations of Crystallography," 1948. [Online]. Available: http://journals.iucr.org/a/journalhomepage.html.

[17] W. G. Wyckoff, *Crystal Structure*, 2nd ed. New-York, 1965, p. 981.

[18] L. Gracia, A. Beltran, A. Franco, and J. Recio, "No Title," *Phys. Rev B*, vol. 66, 2002.

[19] I. B. Bersuker, *Electronic Structure and Properties of Transition Metal Compounds: Introduction to the Theory (Google eBook)*. John Wiley & Sons, 2010, p. 759.

[20] G. Lawes and G. Srinivasan, "Introduction to magnetoelectric coupling and multiferroic films," *J. Phys. D. Appl. Phys.*, vol. 44, no. 24, p. 243001, Jun. 2011.

[21] J. Schwarzkopf and R. Fornari, "Epitaxial growth of ferroelectric oxide films," *Prog. Cryst. Growth Charact. Mater.*, vol. 52, no. 3, pp. 159–212, Sep. 2006.

[22] J. Li, P. Li, and J. Yu, "Study on Substitution Effect of Bi 4 Ti 3 O 12 Ferroelectric Thin Films," 2006.

[23] E. C. Subbarao, "A family of ferrolectric bismuth compounds," *J. Phys. Chem. Solids*, vol. 23, no. 6, pp. 665–676, 1962.

[24] R. Machado, M. G. S. R. L. Migoni, A. H. Tera, and D. De F, "Estructura electr ´ onica y origen de la ferroelectricidad en el Bi 4 Ti 3 O 12 , por medio de c ´ alculos de primeros principios," vol. 51, no. 2, pp. 186–192, 2005.

[25] M. Yamaguchi and T. Magamoto, "Effect of Grain Size on Bi4Ti3O12 Thin Film Propertie," *Jpn. J. Appl. Phys*, vol. 37, pp. 5166–5170, 1998.

[26] T. K. Y. Noguchi, M. Miyayama, "No Title," *Phys. Rev. B*, vol. 63, 2001.

[27] H. I. Rie, M. M. Iyayama, and T. K. Udo, "Domain Motion in Bismuth-Layer-Structured Ferroelectrics by Applying Electric Fields," vol. 38, no. 10, pp. 5958–5963, 1999.

[28] A. Pignolet, C. Schäfer, K. M. Satyalakshmi, C. Harnagea, D. Hesse, and U. Gösele, “Orientation dependence of ferroelectricity in pulsed-laser-deposited epitaxial bismuth-layered perovskite thin films,” 2000.

[29] R. R. Das, P. Bhattacharya, W. Pérez, R. S. Katiyar, and S. B. Desu, “Ferroelectric properties of laser-ablated Sr[sub 1−x]A[sub x]Bi[sub 2]Ta[sub 2]O[sub 9] thin films (where A=Ba, Ca),” *Appl. Phys. Lett.*, vol. 80, no. 4, p. 637, Jan. 2002.

[30] T. Watanabe, H. Funakubo, M. Osada, Y. Noguchi, and M. Miyayama, “Effect of cosubstitution of La and V in Bi[sub 4]Ti[sub 3]O[sub 12] thin films on the low-temperature deposition,” *Appl. Phys. Lett.*, vol. 80, no. 1, p. 100, Jan. 2002.

[31] T. Watanabe, H. Funakubo, M. Mizuhira, and M. Osada, “Site definition and characterization of La-substituted Bi[sub 4]Ti[sub 3]O[sub 12] thin films prepared by metalorganic chemical vapor deposition,” *J. Appl. Phys.*, vol. 90, no. 12, p. 6533, Dec. 2001.

[32] X. Du, J. Zheng, U. Belegundu, and K. Uchino, “Crystal orientation dependence of piezoelectric properties of lead zirconate titanate near the morphotropic phase boundary,” *Appl. Phys. Lett.*, vol. 72, no. 19, p. 2421, May 1998.

[33] M. Budimir, D. Damjanovic, and N. Setter, “Piezoelectric anisotropy–phase transition relations in perovskite single crystals,” *J. Appl. Phys.*, vol. 94, no. 10, p. 6753, Nov. 2003.

[34] H. Nagata, T. Takahashi, Y. Yano, and T. Takenaka, “No Title,” *Ferroelectrics*, vol. 261, 2001.

[35] K.-T. Kim and C.-I. Kim, “The effect of orientation on structure and ferroelectric properties of Bi3.25La0.75Ti3O12 thin films,” *Surf. Coatings Technol.*, vol. 177–178, pp. 770–773, Jan. 2004.

[36] C. S. Ganpule, V. Nagarajan, S. B. Ogale, A. L. Roytburd, E. D. Williams, and R. Ramesh, “Domain nucleation and relaxation kinetics in ferroelectric thin films,” *Appl. Phys. Lett.*, vol. 77, no. 20, p. 3275, Nov. 2000.

[37] A. Sharma, “Pyroelectric response of ferroelectric thin films,” *J. Appl. Phys.*, vol. 95, no. 7, p. 3618, Apr. 2004.

[38] A. F. Chow, D. J. Lichtenwalner, R. R. Woolcott, T. M. Graettinger, O. Auciello, A. I. Kingon, L. A. Boatner, and N. R. Parikh, “Epitaxial KNbO3 thin films on KTaO3, MgAl2O4, and MgO substrates,” *Appl. Phys. Lett.*, vol. 65, no. 9, p. 1073, Aug. 1994.

[39] K. Ishikawa, H. Funakubo, K. Saito, T. Suzuki, Y. Nishi, and M. Fujimoto, “Crystal structure and electrical properties of epitaxial SrBi[sub 2]Ta[sub 2]O[sub 9] films,” *J. Appl. Phys.*, vol. 87, no. 11, p. 8018, Jun. 2000.

[40] V. Srikant, E. J. Tarsa, D. R. Clarke, and J. S. Speck, “Crystallographic orientation of epitaxial BaTiO3 films: The role of thermal-expansion mismatch with the substrate,” *J. Appl. Phys.*, vol. 77, no. 4, p. 1517, Feb. 1995.

[41] T. Watanabe, A. Saiki, K. Saito, and H. Funakubo, “Film thickness dependence of ferroelectric properties of c-axis-oriented epitaxial Bi[sub 4]Ti[sub 3]O[sub 12] thin films prepared by metalorganic chemical vapor deposition,” *J. Appl. Phys.*, vol. 89, no. 7, p. 3934, Apr. 2001.

[42] N. a. Hill, “D Ensity F Unctional S Tudies of M Ultiferroic M Agnetoelectrics,” *Annu. Rev. Mater. Res.*, vol. 32, no. 1, pp. 1–37, Aug. 2002.

[43] N. A. Hill and A. Filippetti, “Why are there any magnetic ferroelectrics?,” *J. Magn. Magn. Mater.*, vol. 242–245, pp. 976–979, Apr. 2002.

[44] H. Schmid, “Magnetic ferroelectric materials,” *Bull. Mater. Sci.*, vol. 17, no. 7, pp. 1411–1414, Dec. 1994.

[45] E. Ascher, “Some Properties of Ferromagnetoelectric Nickel-Iodine Boracite, Ni3B7O13I,” *J. Appl. Phys.*, vol. 37, no. 3, p. 1404, Mar. 1966.

[46] Q. Huang, A. Santoro, J. W. Lynn, R. W. Erwin, J. A. Borchers, J. L. Peng, and R. L. Greene, “Structure and magnetic order in undoped lanthanum manganite,” *Phys. Rev. B*, vol. 55, no. 22, pp. 14987–14999, Jun. 1997.

[47] J. AKIMITSU, H. ICHIKAWA, N. EGUCHI, T. MIYANO, M. NISHI, and K. KAKURAI, “Direct observation of orbital ordering in YTiO3 by means of the polarized neutron diffraction technique,” *J. Phys. Soc. Japan*, vol. 70, no. 12, pp. 3475–3478.

[48] G. A. Smolensky, A. I. Agranovskaya, and V. A. Isupov, “No Title,” *Sov. Phys. Solid State*, vol. 1, no. 149, 1959.

[49] W. Brixel, J. P. Rivera, A. Steiner, and S. H., “No Title,” *Ferroelectrics*, vol. 79, p. 201, 1988.

[50] D. N. Astrov, B. I. Al’shin, Y. Y. Tomashpol’skii, and Y. N. Venevtsev, “No Title,” *Sov. Phys. JETP*, vol. 28, p. 1123, 1969.

[51] M. H. Tsai, Y. H. Tang, and S. K. Dey, “No Title,” *J. Phys. Condens. Matter*, vol. 15, no. 7901, 2003.

[52] M. S. Tomar, R. Melgarejo, S. P. Singh, and R. S. Katiyar, “Bi-functional memories in new electroceramics.”

[53] D. Zhou, G. Jian, Y. Zheng, S. Gong, and F. Shi, “Electrophoretic deposition of BaTiO3/CoFe2O4 multiferroic composite films,” *Appl. Surf. Sci.*, vol. 257, no. 17, pp. 7621–7626, Jun. 2011.

[54] S.-T. Zhang, Y. Zhang, Z.-L. Luo, M.-H. Lu, Z.-B. Gu, and Y.-F. Chen, “Multiferroic properties of Bi0.8La0.2FeO3/CoFe2O4 multilayer thin films,” *Appl. Surf. Sci.*, vol. 255, no. 9, pp. 5092–5095, Feb. 2009.

[55] X. J. Xing, Y. P. Yu, L. M. Xu, Y. L. Zhang, and S. W. Li, “Preparation and magnetic properties of BiFeO3 films in trilayered Bi3.25La0.75Ti3O12/BiFeO3/Bi3.25La0.75Ti3O12 structures,” *Mater. Sci. Eng. B*, vol. 147, no. 1, pp. 95–99, Jan. 2008.

[56] J. Wu and J. Wang, “Multiferroic and Fatigue Behavior of (Bi[sub 0.90]La[sub 0.10])FeO[sub 3]/CoFe[sub 2]O[sub 4]/(Bi[sub 0.90]La[sub 0.10])FeO[sub 3] Sandwich Structure,” *Electrochem. Solid-State Lett.*, vol. 12, no. 10, p. G61, 2009.

[57] S. W. Yi, S. S. Kim, J. W. Kim, H. K. Jo, and D. Do, “Multiferroic properties of BiFeO3/Bi4Ti3O12 double-layered thin films fabricated by chemical solution deposition,” *Thin Solid Films*, vol. 517, no. 24, pp. 6737–6741, Oct. 2009.

[58] X. Tang, J. Dai, X. Zhu, W. Song, and Y. Sun, “Magnetic annealing effects on multiferroic BiFeO3/CoFe2O4 bilayered films,” *J. Alloys Compd.*, vol. 509, no. 14, pp. 4748–4753, Apr. 2011.

[59] B. E. Warren, *X-ray Diffraction*. 1990, pp. 45–48.

[60] “Vibrating Sample Magnetometers | Overview | Lake Shore Cryotronics, Inc.” [Online]. Available: http://www.lakeshore.com/products/Vibrating-Sample-Magnetometer/7400-Series-VSM/Pages/Overview.aspx. [Accessed: 01-Oct-2013].

[61] K. Kwan Chi, *Dielectric Phenomena in Solids*, Elsevier. California, 2004.

[62] J. Goldstein, *Scanning electron microscopy and x-ray microanalysis*, Kluwer Aca. 2003, p. 689.

[63] R. F. Egerton, *Physics principles of electron microscopy: an TEM, SEM and EAM*. 2005, p. 202.

[64] K.-T. Kim and C.-I. Kim, “Effect of bismuth excess on the crystallization of Bi3.25La0.75Ti3O12 thin films on Pt/Ti/SiO2/Si substrates,” *Microelectron. Eng.*, vol. 71, no. 3–4, pp. 266–271, May 2004.

[65] K.-T. Kim and C.-I. Kim, “Characterization of ferroelectric Bi3.25La0.75Ti3O12 thin films prepared by metal organic decomposition method,” *Thin Solid Films*, vol. 478, no. 1–2, pp. 6–12, May 2005.

[66] H. Search, C. Journals, A. Contact, M. Iopscience, and I. P. Address, “The temperature dependence of dielectric dispersion in polycrystalline chromites,” vol. 477, pp. 4–11.